

A TENSOR-TRAIN REDUCED BASIS SOLVER FOR PARAMETERIZED PARTIAL DIFFERENTIAL EQUATIONS

NICHOLAS MUELLER[†], YIRAN ZHAO[‡], SANTIAGO BADIA[†], AND TIANGANG CUI[¶]

ABSTRACT. In this manuscript we present the tensor-train reduced basis method, a novel projection-based reduced-order model for the efficient solution of parameterized partial differential equations. Despite their popularity and considerable computational advantages with respect to their full order counterparts, reduced-order models are typically characterized by a considerable offline computational cost. The proposed approach addresses this issue by efficiently representing high dimensional finite element quantities with the tensor train format. This method entails numerous benefits, namely, the smaller number of operations required to compute the reduced subspaces, the cheaper hyper-reduction strategy employed to reduce the complexity of the PDE residual and Jacobian, and the decreased dimensionality of the projection subspaces for a fixed accuracy. We provide a posteriori estimates that demonstrate the accuracy of the proposed method, we test its computational performance for the heat equation and transient linear elasticity on three-dimensional Cartesian geometries.

1. INTRODUCTION

Projection based reduced order models (ROMs) are classes of numerical methods that approximate parametric high fidelity (HF) models, generally involving fine spatio-temporal discretizations of partial differential equations (PDEs). They aim to approximate the HF parameter-to-solution manifold on a suitably chosen vector subspace. Such models are characterized by a computationally intensive offline phase, where the subspace is computed, and where the (Petrov-)Galerkin projection of the HF equations onto the subspace takes place. Oftentimes, the hyper-reduction of nonaffinely parameterized HF quantities (residuals, Jacobians) also occurs in this step. Then, a cheap online phase providing accurate solutions for new selections of parameters follows.

Space-time ROMs have recently been proposed to simultaneously reduce the spatial and temporal complexity of the full order model (FOM). The space-time reduced basis (ST-RB), firstly proposed in [1] to solve a linear 2d Boltzmann transport equation, is arguably the most important exponent of such methods. This procedure builds a dataset of HF solutions (snapshots), from which it extracts a spatial subspace and a temporal one. Then, it considers as projection space the Kronecker product of said subspaces, on which the FOM residual is minimized under a suitable norm. ST-RB was then extended in [2], where a more relevant 3d Stokes equation is considered. In [3], the authors propose various hyper-reduction strategies in the same space-time framework provided by ST-RB. The accuracy of the resulting methods exhibit the same convergence rates as their more widely-used space-only counterparts [4–7].

In this work we develop a novel ST-RB method called tensor train reduced basis (TT-RB), which employs the recently proposed tensor train (TT) technique for tensor decompositions. In standard ST-RB approaches, the HF snapshots are continuously unfolded in a spatial matrix, or a temporal one, via a reshaping operation. The column space of the spatial matrix represents the spatial evolution of the HF variable, for a fixed time and parameter. This matrix is used to compute the spatial reduced subspace. Conversely, the columns of the temporal matrix represent the temporal evolution of the HF variable, for a fixed spatial coordinate and parameter, and is used to compute the temporal reduced subspace. The subspaces are typically found by employing a direct method such as the truncated proper orthogonal decomposition (TPOD), even though a greedy algorithm [4, 8, 9] can be used. This procedure can be likened to a Tucker decomposition [10–12] of the snapshots, provided one envisions them as a tensor whose axes correspond to the spatial, temporal, and parametric entries of the data. This tensor representation is the same we employ in TT-RB, and we identify a joint spatio-temporal subspace by means of a TT decomposition [13–15] of the snapshots. The TT format representation of a tensor is typically found by using one of two strategies. The first one is called tensor train SVD (TT-SVD) [13, 14], which consists of a successive application of TPODs on different matrix unfoldings of (parts of) the snapshots tensor; the second one is the tensor train cross (TT-CROSS) approach [13, 15, 16], which greedily assembles the TT decomposition via alternating linear schemes [17] and CUR approximation [18]. The former achieves better accuracy but is more costly to run, compared to the latter.

The main benefit of employing TT-RB over a standard ST-RB is the improved efficiency while achieving a similar accuracy, particularly during the offline phase. As we explain in detail in the course of the paper, the main source of efficiency is the implementation of the so-called “split-axis” format of the snapshots, which consists in decomposing the spatial evolution of the snapshots in each Cartesian direction. When working on a Cartesian geometry as we do in this work, the “split-axis” representation is straightforward to derive. On a generic geometry, it could be artificially retrieved

[†]SCHOOL OF MATHEMATICS, MONASH UNIVERSITY, CLAYTON, VICTORIA 3800, AUSTRALIA

[‡]SCHOOL OF MATHEMATICS AND STATISTICS, UNIVERSITY OF SYDNEY, NEW SOUTH WALES 2006, AUSTRALIA

Date: December 20, 2024.

by employing unfitted element discretizations [19], even though we leave this research line for future work. The “split-axis” strategy has the effect of limiting the cost of operations involving spatial quantities, which are typically far larger than temporal and parametric ones. However, using such strategy in standard ST-RB methods would greatly increase the dimension of the reduced subspaces, and thus hurting the online performance of the algorithms. Another intrinsic advantage of TT decompositions is that the accuracy of the reduced basis (RB) approximation is, for a fixed dimension of the reduced subspace, far superior compared to ST-RB. This allows us to seek our reduced approximations on subspaces of very small dimension, and still retain good accuracy.

The purpose of our work is to achieve a projection-based ROM for the efficient approximation of parametric, possibly transient PDEs that are reducible according to the definitions in [4, 20]. Such ROM is built in order to rely exclusively on the computation of TT decompositions of HF quantities, and performing operations on such decompositions. The main contributions of the paper are the following:

- (1) We propose a novel TT-SVD algorithm for the efficient construction of a projection subspace characterized by a non-standard orthogonality condition, for example with respect to the norm induced by an inner product. In contrast, a standard TT-SVD approach returns a basis that is orthogonal in the Euclidean norm. We provide a detailed comparison between the proposed algorithm and the basis construction via TPOD, in terms of cost and accuracy.
- (2) We introduce a new hyper reduction strategy in a TT framework, namely the tensor train MDEIM (TT-MDEIM). In contrast to the standard empirical interpolation method in matrix form (MDEIM), this method empirically interpolates a tensor in its TT format. In our algorithm, we run TT-MDEIM to affinely decompose the residual and jacobian of the problems we consider. We demonstrate that TT-MDEIM achieves essentially the same accuracy as MDEIM.
- (3) We provide *a priori* error estimates for the method that results from combining (1) and (2), which we refer to as the TT-RB method. We show that the accuracy of the procedure is closely linked to a user-defined tolerance, which controls the accuracy of the TT subspace, and of the TT-MDEIM approximation.
- (4) We investigate the numerical properties of the proposed approach by solving two numerical tests, namely a heat equation and an unsteady linear elasticity problem. Both tests are conducted on 3d Cartesian geometries, and feature nonaffine parameterizations affecting their left hand side (LHS) and right hand side (RHS).

This article is organized as follows. In Sect. 2, we provide the notation we employ throughout our work, and we briefly review the main properties of TT decompositions. In Sect. 3, we introduce the FOM given by a parameterized heat equation, and we discuss the basic implementation of the ST-RB approach. In Sect. 4, we propose our novel TT-RB strategy. Here, we detail the construction of the TT reduced subspace, the TT hyper-reduction strategy, and the FOM projection onto said subspace. We discuss the computational cost and *a priori* error estimates associated to these steps. In Sect. 5, we state the TT-RB method we employ to solve the linear elasticity problem. In Sect. 6, we discuss the numerical results obtained when applying the TT-RB method to our test cases. Finally, in Sect. 7 we draw some conclusions and discuss the possible extensions of our work.

2. NOTATION

The notation we employ in the paper draws inspiration from that of [3]. We make use of multidimensional arrays (tensors) storing space-, time-, and parameter-dependent quantities. We use subindices s , t and μ to denote the spatial, temporal and parametric axes. Since we deal with Cartesian geometries, in the course of this work we decompose the spatial axis into the d Cartesian axes. We employ the subindices $1, \dots, d$ to refer to each separate spatial axis. Additionally, we employ the superindex μ to indicate quantities that depend upon an unknown value of the parameter. In this work, the parameters we consider are p -dimensional vectors that are sampled according to a uniform distribution on a given space of parameters. We refer to a generic parameter as $\boldsymbol{\mu} \in \mathbb{R}^p$.

In the two-dimensional case, we have $\mathbf{U}_1^\mu \in \mathbb{R}^{N_1}$, $\mathbf{U}_2^\mu \in \mathbb{R}^{N_2}$ and $\mathbf{U}_t^\mu \in \mathbb{R}^{N_t}$ to be the parameter-dependent vectors in the first spatial space \mathbf{U}_1^μ , the second spatial space \mathbf{U}_2^μ and the temporal space \mathbf{U}_t^μ , respectively. Their tensor product $\mathbf{U}_{1,2,t}^\mu = \mathbf{U}_1^\mu \otimes \mathbf{U}_2^\mu \otimes \mathbf{U}_t^\mu$ is an element in the parameter-dependent tensor product space $\mathcal{U}_{1,2,t}^\mu = \mathcal{U}_1^\mu \otimes \mathcal{U}_2^\mu \otimes \mathcal{U}_t^\mu$.

For the sake of notation, we do not make a distinction between two tensors that are congruent by isometry. For example, if we consider a tensor $\mathbf{U}_{1,2,t,\mu} \in \mathbb{R}^{N_1 \times N_2 \times N_t \times N_\mu}$, we can perform a permutation of axes $\mathbf{U}_{2,1,\mu,t} \in \mathbb{R}^{N_2 \times N_1 \times N_\mu \times N_t}$ or a merging of axes $\mathbf{U}_{12,t,\mu} \in \mathbb{R}^{N_{12} \times N_t \times N_\mu}$, with $N_{12} = N_1 N_2$, without changing the entries of the original tensor. For convenience, we define $N_s = \prod_{i=1}^d N_i$, where the subindex s denotes the merging of the spatial axes.

The aim of our research is to exploit low-rank approximations of solution manifolds to build an efficient ROM solver for PDEs. This amounts to finding a subspace of $\mathcal{U}_{1,2,t}^\mu$ that well describes its elements. In the course of this work, we denote a low-rank approximations with the $\hat{\cdot}$ symbol, e.g. $\hat{\mathbf{U}}_{1,2,t}^\mu \approx \mathbf{U}_{1,2,t}^\mu$. The low-rank approximant $\hat{\mathbf{U}}_{1,2,t}^\mu$ belongs to a reduced subspace spanned by a certain reduced basis, which we seek in a TT format. Let us fix the value of the parameter $\boldsymbol{\mu} = \boldsymbol{\mu}_*$. Moreover, let us introduce the cores of the TT decomposition

$$\boldsymbol{\Phi}_{0,1,\hat{1}}^{\mu_*} \in \mathbb{R}^{r_0 \times N_1 \times r_1}, \quad \boldsymbol{\Phi}_{1,2,\hat{2}}^{\mu_*} \in \mathbb{R}^{r_1 \times N_2 \times r_2}, \quad \boldsymbol{\Phi}_{2,t,\hat{t}}^{\mu_*} \in \mathbb{R}^{r_2 \times N_t \times r_t}, \quad (1)$$

of ranks r_1 , r_2 and r_t , respectively. The first and last sizes are trivial, i.e. $r_0 = r_t = 1$. As we discuss in Sect. 4, the cores (1) are computed by applying on $\mathbf{U}_{1,2,t}^{\mu_*}$ any low-rank approximation available within the TT framework. The TT

approximation of $U_{1,2,t}^{\mu^*}$ reads as:

$$U_{12t}^{\mu^*} \approx \widehat{U}_{12t}^{\mu^*} = \sum_{\alpha_0=1}^{r_0} \sum_{\alpha_1=1}^{r_1} \sum_{\alpha_2=1}^{r_2} \sum_{\alpha_t=1}^{r_t} \Phi_{0,1,\widehat{1}}^{\mu^*}[\alpha_0, :, \alpha_1] \otimes \Phi_{1,2,\widehat{2}}^{\mu^*}[\alpha_1, :, \alpha_2] \otimes \Phi_{2,t,\widehat{t}}^{\mu^*}[\alpha_2, :, \alpha_t]. \quad (2)$$

In essence, the TT format consists in writing (an approximation of) the entries of a d -dimensional tensor in terms of d TT cores. This representation is particularly advantageous for large values of d , since the storage of the TT decomposition scales only linearly with d (and quadratically in the ranks). The quality of the approximation is closely related to the ranks. Low-rank algorithms are designed to compute the TT cores by evaluating an accuracy measure as a function of the rank, and to select the smallest rank such that the accuracy is better than a given threshold. Assuming that the input tensor is reducible [4] and the chosen threshold is not too small, we have $r_i \ll N_i$. For this reason, we refer to the ranks as the reduced ranks (or reduced dimensions) of the TT decomposition (2), and we employ the subindex \widehat{i} to represents r_i . Fig. 1 provides a graphical representation of the intrinsic meaning of (2).

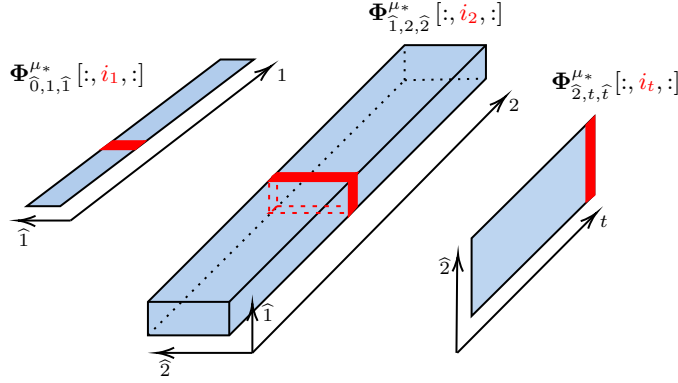


FIGURE 1. Example displaying how the entry $U_{1,2,t}^{\mu^*}[i_1, i_2, i_t]$ is expressed in terms of the TT cores. Firstly, we compute the vector-matrix multiplication between the first and second cores, evaluated at the appropriate indices; then, the resulting row vector is multiplied by the column vector associated to the third core, evaluated at the appropriate index. The resulting scalar corresponds to the desired entry.

We can equivalently express (2) by omitting the sums over the indices i_0 and i_t , and thus the subindices $\widehat{0}$ and \widehat{t} . For this reason, the final subspace $U_{12t}^{\mu^*}$ contains only one element, that is $U_{12t}^{\mu^*}$. In order to simplify the notation of (2), we introduce the product

$$(U_{a,b,c} U_{c,d,e})[\alpha_a, \alpha_b, \alpha_d, \alpha_e] = \sum_{\alpha_c} U_{a,b,c}[\alpha_a, \alpha_b, \alpha_c] U_{c,d,e}[\alpha_c, \alpha_d, \alpha_e]. \quad (3)$$

This operation can be generalized to multiple dimensions, for example

$$(U_{a,b,c,d} U_{e,b,f,d})[\alpha_a, \alpha_c, \alpha_e, \alpha_f] = \sum_{\alpha_b, \alpha_d} U_{a,b,c,d}[\alpha_a, \alpha_b, \alpha_c, \alpha_d] U_{e,b,f,d}[\alpha_e, \alpha_b, \alpha_f, \alpha_d]. \quad (4)$$

In order to sequentially apply (3) on the TT cores, we merge the 2nd and 3rd axes of the 4-d output, so that the result is still a 3d array. This way, we can compactly write (2) as

$$U_{12t}^{\mu^*} = \Phi_{0,1,\widehat{1}}^{\mu^*} \Phi_{1,2,\widehat{2}}^{\mu^*} \Phi_{2,t,\widehat{t}}^{\mu^*}.$$

When one (or more) of the dimensions of the 3d arrays is trivial, we can also employ the product (3) between arrays that are not necessarily 3d, e.g.

$$\Phi_{12,\widehat{2}}^{\mu^*} = \Phi_{1,\widehat{1}}^{\mu^*} \Phi_{1,2,\widehat{2}}^{\mu^*} \cong \Phi_{0,12,\widehat{2}}^{\mu^*}.$$

For the sake of simplicity we do not employ the bold indices notation discussed above for standard matrix-matrix and matrix-vector products, even though these operations are special instances of (4). In general, we reserve the bold indices notation for products involving at least one tensor whose order is larger than two.

The TT decomposition can be understood as an instance of hierarchical format for tensors. Indeed, the TT cores recursively define a basis for $U_{12t}^{\mu^*}$ as

$$U_1^{\mu^*} = \text{col}(\Phi_{0,1,\widehat{1}}^{\mu^*}); \quad U_{12}^{\mu^*} = \text{col}(\Phi_{0,1,\widehat{1}}^{\mu^*} \Phi_{1,2,\widehat{2}}^{\mu^*}); \quad U_{12t}^{\mu^*} = \text{col}(\Phi_{0,1,\widehat{1}}^{\mu^*} \Phi_{1,2,\widehat{2}}^{\mu^*} \Phi_{2,t,\widehat{t}}^{\mu^*}), \quad (5)$$

where col denotes the column space of a matrix.

A TT approximation of $U_{12t}^{\mu^*}$ can be thus found according to the following steps.

- We build a tensor of snapshots $U_{1,2,t,\mu}$, for N_μ different selections of the parameter (note that we do not use the superindex μ here, since we assume the number of sampled parameters to adequately cover the space of parameters).

- We compute the cores $\Phi_{\hat{0},1,\hat{1}}, \Phi_{\hat{1},2,\hat{2}}, \Phi_{\hat{2},t,\hat{t}}$ spanning the RB subspace $\mathcal{U}_{12t}^{\mu*}$ by performing a TT decomposition for $U_{1,2,t,\mu}$, and without caring to compute a parametric core $\Phi_{\hat{t},\mu,\hat{\mu}}$. Note that the dimension of our RB space is equal to the temporal rank r_t , which is no longer necessarily equal to 1.
- For any μ_* , we have the approximation

$$U_{1,2,t}^{\mu*} \approx \hat{U}_{1,2,t}^{\mu*} = \Phi_{\hat{0},1,\hat{1}} \Phi_{\hat{1},2,\hat{2}} \Phi_{\hat{2},t,\hat{t}} \hat{U}_{\hat{t}}^{\mu*},$$

where $\hat{U}_{\hat{t}}^{\mu*}$ is the vector of coordinates associated to $U_{1,2,t}^{\mu*}$ in the TT basis. As we will discuss in the following section, we treat this (reduced) vector of coefficients as the unknown of the TT-RB method.

Lastly, we establish a multi-axes notation to concisely deal with tensors of generic sizes. For example, $U_{1,\dots,d,t,\mu}$ when d is not necessarily 2. We represent the axes of the tensor starting from i with the multi-axes $\gamma_i = (i, i+1, \dots, t, \mu)$. This way, we can write

$$U_{1,\dots,d,t,\mu} = U_{\gamma_1} = U_{1,\gamma_2} = \dots = U_{1,\dots,d,\gamma_t}. \quad (6)$$

When merging multiple axes we resort to the symbol γ_i . For example, we can compactly express $U_{1,\dots,d,t,\mu}$ as U_{γ_1} , and so on. We can exploit the multi-axes notation to indicate sizes, e.g. $N_{\gamma_1} = N_1 \cdots N_d N_t$. Also note that, according to the definition (6), the temporal axis t can also be indicated with the subindex $d+1$.

3. REDUCED BASIS METHOD IN SPACE TIME

We begin this section by introducing the FOM given by a parameterized heat equation on a d -cube. Then, we provide an overview of the ST-RB method applied to the FOM.

3.1. Full order model. We consider a d -cube $\Omega = \Omega_1 \times \dots \times \Omega_d$ with boundary $\partial\Omega$, a temporal domain $[0, T] \subset \mathbb{R}_+ \cup \{0\}$, and a parameter space $\mathcal{D} \subset \mathbb{R}^p$. Given $\mu \in \mathcal{D}$, a generic heat equation defined on the space-time domain $\Omega \times [0, T]$ reads:

$$\begin{cases} \frac{\partial u^\mu}{\partial t} - \nabla \cdot (\alpha^\mu \nabla u^\mu) = f^\mu & \text{in } \Omega \times (0, T], \\ u^\mu = g^\mu & \text{on } \Gamma_D \times (0, T], \\ \alpha^\mu \underline{n} \cdot \nabla u^\mu = h^\mu & \text{on } \Gamma_N \times (0, T], \\ u^\mu = u_0^\mu & \text{in } \Omega \times \{0\}, \end{cases} \quad (7)$$

where $u^\mu : \Omega \times [0, T] \rightarrow \mathbb{R}$ is the unknown state variable. Such variable is implicitly μ -dependent through the parametric heat diffusivity $\alpha^\mu : \Omega \times [0, T] \rightarrow \mathbb{R}_+$, forcing term $f^\mu : \Omega \times [0, T] \rightarrow \mathbb{R}$, Dirichlet and Neumann data $g^\mu : \Gamma_D \times [0, T] \rightarrow \mathbb{R}$, $h^\mu : \Gamma_N \times [0, T] \rightarrow \mathbb{R}$, and initial condition $u_0^\mu : \Omega \rightarrow \mathbb{R}$. We additionally define the Dirichlet and Neumann boundaries Γ_D and Γ_N , such that $\{\Gamma_D, \Gamma_N\}$ forms a partition of $\partial\Omega$. Moreover, we assume for simplicity that Γ_D can be written as the union of entire legs of the d -cube, i.e. any element of Γ_D coincides with an entire $d-1$ -dimensional facet of $\partial\Omega$. We remark that this assumption does not represent a loss of generality, and we use it only to present the analysis of the FOM while imposing the Dirichlet conditions strongly. If the aforementioned condition does not hold, we simply consider a weak imposition of the Dirichlet datum, e.g. with a Nitsche penalty method [21, 22].

Now we introduce a conforming quasi-uniform quadrangular partition of Ω , denoted as \mathcal{T}_h , and a uniform partition of $[0, T]$, namely $\{t_n\}_{n=0}^{N_t}$. The former is the spatial mesh, with h a parameter indicating its size; the latter is the temporal mesh, such that $t_n = n\delta$, where $\delta = T/N_t$ is the time-step size. Note that \mathcal{T}_h can be written as the tensor product of 1-d partitions defined on $\Omega_1, \dots, \Omega_d$, a fact we will continuously exploit in the course of this work. For the spatial discretization of (7), we consider the Hilbert spaces

$$\mathcal{V} = H^1(\Omega); \quad \mathcal{V}_{\Gamma_D}^0 = \{v \in H^1(\Omega) : v = 0 \text{ on } \Gamma_D\},$$

and their finite-dimensional counterparts $\mathcal{V}_h \subset \mathcal{V}$ on \mathcal{T}_h , and $\mathcal{V}_h^0 = \mathcal{V}_h \cap \mathcal{V}_{\Gamma_D}^0$. For the time discretization, we consider the Backward Euler (BE) scheme for simplicity of the exposition, even though a Crank-Nicolson method is used in our numerical tests. In this work, we impose the Dirichlet boundary conditions strongly, i.e. we lift the Dirichlet data, we seek a solution on \mathcal{V}_h^0 , and we retrieve the non-homogeneous solution on \mathcal{V}_h by adding back the lifting term. Upon writing the (lifted) weak formulation of (7), and performing numerical integration, we can algebraically express the FOM as

$$(\delta^{-1} \mathbf{M}_{s,s} + \mathbf{A}_{s,s}^\mu(t_n)) (\mathbf{U}_s^\mu)_n = \mathbf{L}_s^\mu(t_n) + \delta^{-1} \mathbf{M}_{s,s} (\mathbf{U}_s^\mu)_{n-1}, \quad n \in \mathbb{N}(N_t), \quad (8)$$

where $\mathbb{N}(k) = \{1, \dots, k\}$ for any positive integer k . The quantity $(\mathbf{U}_s^\mu)_n \in \mathbb{R}^{N_s}$ is the vector of degrees of freedom (DOFs) of $(u_h^\mu)_n \in \mathcal{V}_h^0$, the finite element (FE) approximation at the time instant t_n with homogeneous Dirichlet values. Thanks to the definitions of Ω and \mathcal{T}_h , the FE basis functions spanning \mathcal{V}_h (and \mathcal{V}_h^0 , by virtue of the assumptions on Γ_D) assume a tensor product structure. In particular, they can be written as the tensor product of FE basis functions defined on the 1-d partitions whose tensor product forms \mathcal{T}_h [23]. Because of the tensor product structure of the FE spaces, we can identify $(\mathbf{U}_s^\mu)_n$ with $(U_{1,\dots,d})_n \in \mathbb{R}^{N_1 \times \dots \times N_d}$. In (8), the symbols $\mathbf{M}_{s,s}$, $\mathbf{A}_{s,s}^\mu$ and \mathbf{L}_s^μ denote the mass matrix (which is independent of t, μ in this work), the stiffness matrix and the RHS vector, respectively. Similarly to the vector of DOFs, we can express the RHS vector as a d -dimensional tensor, and the mass and stiffness matrices as $2d$ -dimensional tensors. We remark that $\mathbf{M}_{s,s}$, $\mathbf{A}_{s,s}^\mu$ are sparse matrices, and as such can be equivalently identified with their vectors of nonzero

entries $M_z, \mathbf{A}_z^\mu \in \mathbb{R}^{N_z}$, where the subindex z refers to the number of nonzero entries N_z . Writing (8) at every time step yields the space-time algebraic system

$$\mathbf{K}_{st,st}^\mu \mathbf{U}_{st}^\mu = \mathbf{L}_{st}^\mu. \quad (9)$$

Here, $\mathbf{K}_{st,st}^\mu$ is a bi-diagonal block-matrix with N_t diagonal blocks $\delta^{-1} \mathbf{M}_{s,s} + \mathbf{A}_{s,s}^\mu(t_i)$, and lower diagonal blocks $\delta^{-1} \mathbf{M}_{s,s}$; the space-time vectors $\mathbf{U}_{st}^\mu, \mathbf{L}_{st}^\mu$ are obtained by simply concatenating vertically their spatial counterparts, for every time step. We also introduce the symmetric, positive definite matrix $\mathbf{X}_{s,s} = \mathbf{A}_{s,s}$, representing the H_0^1 inner product on \mathcal{V}_h^0 , with $\mathbf{A}_{s,s}$ being the discrete Laplacian with unit diffusivity. On a Cartesian mesh, the following property holds:

$$\mathbf{X}_{s,s} = \mathbf{A}_{s,s} = \mathbf{A}_{1,1} \otimes \mathbf{M}_{2,2} \otimes \cdots \otimes \mathbf{M}_{d,d} + \mathbf{M}_{1,1} \otimes \mathbf{A}_{2,2} \otimes \cdots \otimes \mathbf{M}_{d,d} + \dots + \mathbf{M}_{1,1} \otimes \mathbf{M}_{2,2} \otimes \cdots \otimes \mathbf{A}_{d,d}. \quad (10)$$

We can think of $\mathbf{X}_{s,s}$ as a d -rank tensor. Lastly, we define a global spatio-temporal norm matrix $\mathbf{X}_{st,st}$, a block-diagonal matrix with N_t blocks $\delta \mathbf{X}_{s,s}$. The factor δ serves to represent the $L^2(0, T; \mathcal{V})$ product of the FE bases.

3.2. Space-time reduced-basis method. ST-RB is a data driven procedure, consisting of

- (1) An expensive *offline phase*, where the spatio-temporal basis is computed, and the (Petrov-)Galerkin projection of the FOM (9) is obtained.
- (2) A cheap *online phase*, where a RB approximation is returned for any given value of μ .

We introduce two disjoint sets of offline and online parameters, namely $\mathcal{D}_{off} = \{\mu_k\}_{k=1}^{N_\mu} \subset \mathcal{D}$ and $\mathcal{D}_{on} = \{\mu_k\}_{k=1}^{N_\mu} \subset \mathcal{D}$. We compute the (offline) FOM snapshots $\mathbf{U}_{s,t,\mu}$, obtained by solving and storing the solution of (9) for every $\mu_k \in \mathcal{D}_{off}$. (We recall that a standard ST-RB does not employ the aforementioned ‘‘split-axes’’ of the snapshots.) From the snapshots, we extract an $\mathbf{X}_{s,s}$ -orthogonal spatial basis, and an ℓ^2 -orthogonal temporal basis; an $\mathbf{X}_{st,st}$ -orthogonal space-time basis can be obtained as the Kronecker product of the two bases. A standard ST-RB method considers as projection subspace the one spanned by such space-time basis. The procedure is summarized in Alg. 1, along with the computational cost associated to each step.

Algorithm 1 TPOD: Given the tensor of space-time snapshots $\mathbf{U}_{s,t,\mu}$, the prescribed accuracy ε , and the norm matrix $\mathbf{X}_{s,s}$, build the $\mathbf{X}_{s,s}$ -orthogonal spatial basis $\Phi_{s,\hat{s}}$ and the ℓ^2 -orthogonal temporal basis $\Phi_{t,\hat{t}}$.

- 1: **function** TPOD($\mathbf{U}_{s,t,\mu}, \mathbf{X}_{s,s}, \varepsilon$)
 - 2: Cholesky factorization: $\mathbf{H}_{s,s}^T \mathbf{H}_{s,s} = \text{Cholesky}(\mathbf{X}_{s,s})$ $\triangleright \mathcal{O}(N_s^q)$
 - 3: Spatial rescaling: $\tilde{\mathbf{U}}_{s,t,\mu} = \mathbf{H}_{s,s} \mathbf{U}_{s,t,\mu}$ $\triangleright \mathcal{O}(N_z N_t N_\mu)$
 - 4: Spatial reduction: $\tilde{\Phi}_{s,\hat{s}}, \tilde{\mathbf{R}}_{\hat{s},t,\mu} = \text{TSVD}(\tilde{\mathbf{U}}_{s,t,\mu}, \varepsilon)$ $\triangleright \mathcal{O}(N_z (N_t N_\mu)^2)$
 - 5: Spatial inverse rescaling: $\Phi_{s,\hat{s}} = \mathbf{H}_{s,s}^{-1} \tilde{\Phi}_{s,\hat{s}}$ $\triangleright \mathcal{O}(N_z r_s)$
 - 6: Spatial contraction: $\hat{\mathbf{U}}_{\hat{s},t,\mu} = \Phi_{s,\hat{s}} \mathbf{X}_{s,s} \mathbf{U}_{s,t,\mu}$ $\triangleright \mathcal{O}(r_s N_s N_t N_\mu + N_z N_t N_\mu)$
 - 7: Temporal reduction: $\Phi_{t,\hat{t}}, \mathbf{R}_{\hat{t},\hat{s}\mu} = \text{TSVD}(\hat{\mathbf{U}}_{\hat{s},t,\mu}, \varepsilon)$ $\triangleright \mathcal{O}(\min\{N_t (r_s N_\mu)^2, r_s N_\mu N_t^2\})$
 - 8: Return $\Phi_{s,\hat{s}}, \Phi_{t,\hat{t}}$
 - 9: **end function**
-

The two TSVD functions are responsible for finding the r_s -dimensional spatial subspace and the r_t -dimensional temporal one, respectively. We recall in Alg. 2 the details of the procedure.

Algorithm 2 TSVD: Given the matrix $\mathbf{U}_{\alpha,\beta} \in \mathbb{R}^{N_\alpha, N_\beta}$ of rank $N_\sigma = \max\{N_\alpha, N_\beta\}$ and the prescribed accuracy ε , return the orthogonal matrix $\Phi_{\alpha,\hat{\alpha}}$ and the remainder $\mathbf{R}_{\hat{\alpha},\beta}$ truncated at ε .

- 1: **function** TSVD($\mathbf{U}_{\alpha,\beta}, \varepsilon$)
 - 2: Singular value decomposition: $\Phi_{\alpha,\sigma} \Sigma_{\sigma,\sigma} \mathbf{V}_{\sigma,\beta}^T = \text{SVD}(\mathbf{U}_{\alpha,\beta})$
 - 3: Truncation: $r = \arg \min_x \sum_{i=1}^x \Sigma_{\sigma,\sigma} [i, i]^2 / \sum_{i=1}^{N_\sigma} \Sigma_{\sigma,\sigma} [i, i]^2 \geq 1 - \varepsilon^2$
 - 4: Define $\Phi_{\alpha,\hat{\alpha}} = \Phi_{\alpha,\sigma}[:, 1:r]$, $\mathbf{R}_{\hat{\alpha},\beta} = \Sigma_{\sigma,\sigma} [1:r, 1:r] \mathbf{V}_{\sigma,\beta}^T [1:r, :]$
 - 5: Return $\Phi_{\alpha,\hat{\alpha}}, \mathbf{R}_{\hat{\alpha},\beta}$
 - 6: **end function**
-

The selection of the ranks r_s and r_t occurs by means of the well-known relative energy criterion [4]. We remark that the remainder computed by Alg. 2 serves no purpose within Alg. 1. Nonetheless, the TSVD we implement returns this quantity since we will make extensive use of it when running TT-SVD, as we will explain in the next section. The cost estimates in Alg. 1 have been derived considering direct methods, and thanks to the following observations:

- The Cholesky factorization of a $N_s \times N_s$ sparse matrix obtained via numerical integration on a square mesh is $\mathcal{O}(N_s^q)$, where $q = 1$ if $d = 1$, $q = 4/3$ if $d = 2$, and $q = 2$ if $d = 3$ [24, 25].

- The Cholesky factor $\mathbf{H}_{s,s}$ is sparse, with a number of nonzero entries $\sim N_z$. Therefore, the cost of $\mathbf{H}_{s,s}\mathbf{U}_{s,t\mu}$ is $\mathcal{O}(N_z N_t N_\mu)$, and the cost of the singular value decomposition (SVD) is $N_z(N_t N_\mu)^2$, assuming that $N_z > N_t N_\mu$.
- Similarly, the product $\mathbf{H}_{s,s}^{-1}\tilde{\Phi}_{s,\hat{s}}$ requires $\mathcal{O}(N_z r_s)$ operations.
- The spatial contraction is in essence the so-called sequentially truncated high order singular value decomposition (ST-HOSVD) approach [26] to reduce the cost of the temporal compression. Overall, the cost of ST-HOSVD is that of the spatial compression, which comprises two matrix-matrix multiplications, whereas the subsequent SVD becomes negligible in cost. Note that employing ST-HOSVD is optional, and one could instead run an SVD directly on the uncompressed temporal snapshots $\mathbf{U}_{t,s\mu}$, with a cost of $N_s N_\mu N_t^2$. This approach is preferred in the cases where $r_s < N_t$ (which should never occur in practice).

As previously mentioned, ST-RB considers the space-time basis

$$\mathbb{R}^{N_{st} \times r_{st}} \ni \Phi_{st,\hat{st}} = \Phi_{s,\hat{s}} \otimes \Phi_{t,\hat{t}},$$

where $r_{st} = r_s r_t$ is the dimension of the reduced subspace, represented by the subscript \hat{st} . Thus, in TPOD, the dimension of the subspace is given by the product of the dimensions of the spatial and temporal subspaces. (Note that the TT decomposition generates a subspace of dimension equal to that of the temporal subspace only, thanks to the hierarchical relation (5).) We recall the accuracy of the space-time basis:

$$\sum_{j=1}^{N_\mu} \left\| \left(\mathbf{U}_{st,\mu} - \Phi_{st,\hat{st}} \Phi_{\hat{st},st} \mathbf{X}_{st,st} \mathbf{U}_{st,\mu} \right)[:,j] \right\|_{\mathbf{X}_{st,st}}^2 \leq \varepsilon^2 \left(\|\mathbf{U}_{s,t\mu}\|_F^2 + \|\hat{\mathbf{U}}_{t,\hat{s}\mu}\|_F^2 \right). \quad (11)$$

The term $\hat{\mathbf{U}}_{t,\hat{s}\mu}$ appearing in the estimate is the spatial contraction we compute when running ST-HOSVD. The result (11) can be obtained by putting together the contributions of [3], where the proof is made in the case of an ℓ^2 -orthogonal basis, and [4, 5], where the authors establish the relationship between an ℓ^2 -orthogonal basis and an $\mathbf{X}_{st,st}$ -orthogonal one.

We now describe the online phase of ST-RB. Here we must assemble and solve a reduced version of (9). In this work, we consider the reduced equations given by the Galerkin projection of (9) onto the subspace spanned by $\Phi_{st,\hat{st}}$. We refer to [7] for a detailed review of the more general Petrov-Galerkin projections applied to RB methods. Adopting an algebraic notation, the ST-RB problem reads as

$$\text{find } \hat{\mathbf{U}}_{st}^\mu \text{ such that } \Phi_{\hat{st},st} \left(\mathbf{L}_{st}^\mu - \mathbf{K}_{st,st}^\mu \Phi_{st,\hat{st}} \hat{\mathbf{U}}_{st}^\mu \right) = \mathbf{0}_{\hat{st}} \iff \hat{\mathbf{K}}_{st,\hat{st}}^\mu \hat{\mathbf{U}}_{st}^\mu = \hat{\mathbf{L}}_{st}^\mu, \quad (12)$$

where $\hat{\mathbf{K}}_{st,\hat{st}}^\mu = \Phi_{\hat{st},st} \mathbf{K}_{st,st}^\mu \Phi_{st,\hat{st}}$, and $\hat{\mathbf{L}}_{st}^\mu = \Phi_{\hat{st},st} \mathbf{L}_{st}^\mu$ are the Galerkin compression of the space-time LHS and RHS, respectively. Given that computing such quantities heavily relies on operations whose cost scales with the full order dimensions, utilizing a hyper-reduction strategy for the approximation of the Jacobians and residuals is paramount. A hyper-reduction method, such as MDEIM [3, 5], proposes to find the following affine expansions:

$$\mathbf{K}_{st,st}^\mu \approx \Phi_{st,\hat{st}^\mathbf{K}} \mathbf{K}_{st,\hat{st}^\mathbf{K}}^\mu; \quad \mathbf{L}_{st}^\mu \approx \Phi_{st,\hat{st}^\mathbf{L}} \mathbf{L}_{st,\hat{st}^\mathbf{L}}^\mu. \quad (13)$$

Here, $\Phi_{st,\hat{st}^\mathbf{K}} \in \mathbb{R}^{N_{st} \times r_{st}^\mathbf{K} \times N_{st}}$ and $\Phi_{st,\hat{st}^\mathbf{L}} \in \mathbb{R}^{N_{st} \times r_{st}^\mathbf{L}}$ are two bases that span subspaces of reduced dimensions, on which we approximate the manifold of parameterized Jacobians and residuals. The idea is to solve the approximated ROM obtained by plugging the affine expansions (13) in (12):

$$\text{find } \hat{\mathbf{U}}_{st}^\mu \text{ such that } \hat{\mathbf{K}}_{st,\hat{st}}^\mu \hat{\mathbf{U}}_{st}^\mu = \hat{\mathbf{L}}_{st}^\mu, \quad (14)$$

where

$$\hat{\mathbf{K}}_{st,\hat{st}}^\mu \approx \hat{\mathbf{K}}_{st,st}^\mu = \sum_{i=1}^{r_{st}^\mathbf{K}} \Phi_{\hat{st},st} \Phi_{st,\hat{st}^\mathbf{K}} \mathbf{K}_{st,\hat{st}^\mathbf{K}}^\mu[:,i,:]; \quad \hat{\mathbf{L}}_{st}^\mu \approx \hat{\mathbf{L}}_{st}^\mu = \sum_{i=1}^{r_{st}^\mathbf{L}} \Phi_{\hat{st},st} \Phi_{st,\hat{st}^\mathbf{L}} \mathbf{L}_{st,\hat{st}^\mathbf{L}}^\mu[:,i].$$

Given the μ -independence of the bases, we can run offline the bulk of the Galerkin projections. During the online phase, we must only compute the reduced coefficients $\hat{\mathbf{K}}_{st,\hat{st}^\mathbf{K}}^\mu$, $\hat{\mathbf{L}}_{st,\hat{st}^\mathbf{L}}^\mu$, and compute the products with the projected bases. These operations scale exclusively with the reduced sizes r_{st} , $r_{st}^\mathbf{K}$, and $r_{st}^\mathbf{L}$, i.e. they are independent of the FOM dimensions. This allows us to fully exploit the efficient framework that ROMs typically provide. In this work, we consider MDEIM as hyper-reduction strategy. We provide all the necessary details in Subsection 4.2.

4. A NOVEL TT-RB SOLVER

In this section, we discuss the TT-RB method. Here, we still aim to solve the reduced problem (12), but the projection operator is now expressed in a TT format:

$$\Phi_{st,\hat{t}} = \Phi_{0,1,\hat{1}} \cdots \Phi_{d,t,\hat{t}}. \quad (15)$$

We recall that the dimension of the projection subspace is now represented by the axis \hat{t} , instead of \hat{st} as in ST-RB. Indeed, the dimension of a TT subspace is given by the last reduced dimension (see (5) for more details), whereas in

the ST-RB case it is given by the product of the reduced dimensions. The first step is to detail the construction of $\widehat{\Phi}_{st,\hat{t}}$ that satisfies the $\mathbf{X}_{st,st}$ -orthogonality condition, as in the case of TPOD. Secondly, we provide the formal definition of a standard MDEIM procedure and discuss its extension to empirically interpolate TT decompositions, which we refer to as TT-MDEIM. Then, we elaborate a method to project the TT-MDEIM approximation of residuals and Jacobians, solely exploiting operations on the cores. Lastly, we present an accuracy measure for the resulting TT-RB method.

4.1. Basis construction. We consider the FOM snapshots $\mathbf{U}_{s,t,\mu}$ introduced in Sect 3, but this time expressed in the “split axes” format, i.e. $\mathbf{U}_{1,\dots,d,t,\mu}$. A TT decomposition is commonly extracted from the snapshots by running either a TT-SVD or a TT-CROSS strategy. Despite being cheaper, the latter has two drawbacks: the hierarchical bases have a larger rank for a fixed accuracy, and the unavailability of *a priori* error estimates. Moreover, in this work we only deal with snapshots tensors of order 4 (in 2d problems) or 5 (in 3d problems); typically, TT-CROSS is shown to outperform TT-SVD when compressing tensors of order much larger than the ones we must handle. For these reasons, we construct our RB subspaces with the TT-SVD methodology.

We review the TT-SVD algorithm, as presented in [13]. For conciseness, we employ the multi-axes notation in (6).

Algorithm 3 TT-SVD: Given the snapshots tensor in the “split-axes” format \mathbf{U}_{γ_1} and the prescribed accuracy ε , build the TT-cores $\widehat{\Phi}_{0,1,\hat{1}}, \dots, \widehat{\Phi}_{d-1,d,\hat{d}}, \widehat{\Phi}_{\hat{d},t,\hat{t}}$

```

1: function TT-SVD( $\mathbf{U}_{\gamma_1}, \varepsilon$ )
2:   Initialize 1st rank:  $r_0 = 1$ 
3:   Initialize unfolding tensor:  $\mathbf{T}_{\gamma_1} = \mathbf{U}_{\gamma_1}$ 
4:   for  $i = 1, \dots, d$  do
5:      $i$ th spatial reduction:  $\widehat{\Phi}_{i-1,i,\hat{i}} \widehat{\mathbf{R}}_{i,\gamma_{i+1}} = \text{TSVD}(\mathbf{T}_{i-1i,\gamma_{i+1}}, \varepsilon)$ 
6:     Update unfolding tensor:  $\mathbf{T}_{i,\gamma_{i+1}} = \widehat{\mathbf{R}}_{i,\gamma_{i+1}}$ 
7:   end for
8:   Temporal reduction:  $\widehat{\Phi}_{\hat{d},t,\hat{t}} \widehat{\mathbf{R}}_{\hat{t},\mu} = \text{TSVD}(\mathbf{T}_{\hat{d},t,\mu}, \varepsilon)$ 
9:   return  $\widehat{\Phi}_{0,1,\hat{1}}, \dots, \widehat{\Phi}_{d-1,d,\hat{d}}, \widehat{\Phi}_{\hat{d},t,\hat{t}}$ 
10: end function

```

The TT-SVD computes the TT cores by successively applying an SVD on the (truncated) remainder of the previous iteration. Similarly to TPOD, we use the hyper-parameter ε to control the error of the algorithm. In particular, the following statement of accuracy holds (see [13] for more details).

Theorem 1. Suppose the unfolding tensors $\mathbf{T}_{i-1i,\gamma_{i+1}}$ admit a low rank approximation for every i , that is there exist tolerances $\varepsilon_i > 0$ such that:

$$\mathbf{T}_{i-1i,\gamma_{i+1}} = \widehat{\mathbf{R}}_{i-1i,\gamma_{i+1}} + \mathbf{E}_{i-1i,\gamma_{i+1}}, \quad \text{rank}(\widehat{\mathbf{R}}_{i-1i,\gamma_{i+1}}) = r_i, \quad \|\mathbf{E}_{i-1i,\gamma_{i+1}}\|_F^2 = \varepsilon_i^2 \|\mathbf{T}_{i-1i,\gamma_{i+1}}\|_F^2.$$

The following inequality holds:

$$\|\mathbf{U}_{st,\mu} - \widehat{\Phi}_{st,\hat{t}} \widehat{\Phi}_{\hat{t},st} \mathbf{U}_{st,\mu}\|_F^2 \leq \sum_{i=1}^{d+1} \varepsilon_i^2 \|\mathbf{T}_{i-1i,\gamma_{i+1}}\|_F^2 \leq \varepsilon^2 (d+1) \|\mathbf{U}_{st,\mu}\|_F^2,$$

where $\varepsilon = \sup_i \varepsilon_i$

Thm. 1 states that, under an appropriate assumption of reducibility of the snapshots, running the TT-SVD with a modified tolerance $\tilde{\varepsilon} = \varepsilon/\sqrt{d+1}$ yields a basis characterized by the same accuracy as that achieved by the TPOD basis. We also remark that one could also run Alg. 3 on a snapshots tensor with permuted axes, thus obtaining a different reduced subspace. Even though there exists an axes ordering that minimizes the dimension of the output subspace for a fixed ε , in this work we fix the order of the axes according to the multi-axes (6).

In the context of model order reduction of PDEs, a RB satisfying an orthogonality condition in the energy norm of the FE spaces is desirable. Our aim is to modify Alg. 3 so that the resulting TT decomposition is $\mathbf{X}_{st,st}$ -orthogonal. In the following theorem, we state the accuracy of the TT-SVD algorithm when imposing such orthogonality.

Theorem 2. Let $\mathbf{X}_{s,s}$ be a matrix representing a norm on a finite-dimensional subspace of a Hilbert space. Let $\widetilde{\mathbf{U}}_{s,t\mu} = \mathbf{H}_{s,s} \mathbf{U}_{s,t\mu}$, with $\mathbf{H}_{s,s}$ being the upper-triangular Cholesky factor of $\mathbf{X}_{s,s}$. We denote the TT-SVD unfoldings of $\widetilde{\mathbf{U}}_{\gamma_i}$ as $\widetilde{\mathbf{T}}_{i-1i,\gamma_{i+1}}$, which we suppose admit a low rank approximation for every i . In other words, there exist tolerances $\varepsilon_i > 0$ such that:

$$\widetilde{\mathbf{T}}_{i-1i,\gamma_{i+1}} = \widetilde{\mathbf{R}}_{i-1i,\gamma_{i+1}} + \widetilde{\mathbf{E}}_{i-1i,\gamma_{i+1}}, \quad \text{rank}(\widetilde{\mathbf{R}}_{i-1i,\gamma_{i+1}}) = r_i, \quad \|\widetilde{\mathbf{E}}_{i-1i,\gamma_{i+1}}\|_F^2 = \varepsilon_i^2 \|\widetilde{\mathbf{T}}_{i-1i,\gamma_{i+1}}\|_F^2. \quad (16)$$

The following inequality holds:

$$\sum_{j=1}^{N_\mu} \left\| \left(\mathbf{U}_{st,\mu} - \widehat{\Phi}_{st,\hat{t}} \widehat{\Phi}_{\hat{t},st} \mathbf{X}_{st,st} \mathbf{U}_{st,\mu} \right)[:, j] \right\|_{\mathbf{X}_{st,st}}^2 \leq \sum_{i=1}^{d+1} \varepsilon_i^2 \|\widetilde{\mathbf{T}}_{i-1i,\gamma_{i+1}}\|_F^2 \leq \varepsilon^2 (d+1) \|\mathbf{U}_{st,\mu}\|_{\mathbf{X}_{st,st}}^2, \quad (17)$$

where $\varepsilon = \sup_i \varepsilon_i$.

Proof. By virtue of the hierarchical property (5), we can prove the statement (17) by firstly showing

$$\sum_{j=1}^{N_t N_\mu} \left\| \left(\mathbf{U}_{s,t\mu} - \Phi_{s,\hat{d}} \widehat{\Phi}_{\hat{d},s} \mathbf{X}_{s,s} \mathbf{U}_{s,t\mu} \right) [\cdot, j] \right\|_{\mathbf{X}_{s,s}}^2 \leq \sum_{i=1}^d \varepsilon_i^2 \left\| \widehat{\mathbf{T}}_{i-1, \gamma_{i+1}} \right\|_F^2, \quad (18)$$

and secondly proving that the temporal error is of order ε_t . We can run this last step by proceeding as in the proof of Thm. 1, since the temporal norm is the standard euclidean one. We refer to [13] for the complete proof. Therefore, we limit ourselves to demonstrate that (18) holds. Note that:

$$\sum_j \left\| \left(\mathbf{U}_{s,t\mu} - \Phi_{s,\hat{d}} \widehat{\Phi}_{\hat{d},s} \mathbf{X}_{s,s} \mathbf{U}_{s,t\mu} \right) [\cdot, j] \right\|_{\mathbf{X}_{s,s}}^2 = \left\| \widetilde{\mathbf{U}}_{s,t\mu} - \widetilde{\Phi}_{s,\hat{d}} \widetilde{\Phi}_{\hat{d},s} \widetilde{\mathbf{U}}_{s,t\mu} \right\|_F^2, \quad (19)$$

where $\widetilde{\Phi}_{s,\hat{d}} = \mathbf{H}_{s,s} \Phi_{s,\hat{d}}$ (see [4] for more details). By virtue of (16), we can apply Thm. 1 on the tuple $(\widetilde{\mathbf{U}}_{s,t\mu}, \widetilde{\Phi}_{s,\hat{d}})$, and thus

$$\left\| \widetilde{\mathbf{U}}_{s,t\mu} - \widetilde{\Phi}_{s,\hat{d}} \widetilde{\Phi}_{\hat{d},s} \widetilde{\mathbf{U}}_{s,t\mu} \right\|_F^2 \leq \sum_{i=1}^d \varepsilon_i^2 \left\| \widehat{\mathbf{T}}_{i-1, \gamma_{i+1}} \right\|_F^2 \leq \varepsilon^2 (d+1) \left\| \widetilde{\mathbf{U}}_{st,\mu} \right\|_F^2. \quad (20)$$

Therefore, upon selecting the basis $\Phi_{s,\hat{d}} = \mathbf{H}_{s,s}^{-1} \widetilde{\Phi}_{s,\hat{d}}$, and noticing that

$$\left\| \widetilde{\mathbf{U}}_{st,\mu} \right\|_F^2 = \left\| \mathbf{U}_{st,\mu} \right\|_{\mathbf{X}_{st,st}}^2,$$

Eqs. (19) and (20) imply that (18) holds. \square

Therefore, we first pre-multiply the snapshots tensor by the Cholesky factor $\mathbf{H}_{s,s}$. Secondly, we post-multiply the TT basis we extract from the resulting tensor by $\mathbf{H}_{s,s}^{-1}$. This subspace has, in the energy norm, the same approximation capability as the one computed via standard TT-SVD, in the Euclidean norm. Note, however, that both the computation of $\mathbf{H}_{s,s}$ and $\widetilde{\mathbf{U}}_{s,t\mu}$ involve matrices of size $N_s \times N_s$, thus entailing considerable costs. To address this issue, we develop a sequential algorithm by exploiting the ‘‘split-axes’’ principle. We first present the idea in a simplified case $\mathbf{X}_{s,s}$ is a rank-one tensor, i.e., when $\mathbf{X}_{s,s} = \mathbf{M}_{s,s}$, as the mass matrix is indeed rank-1. Then, we elaborate the algorithm for a generic $\mathbf{X}_{s,s}$ of rank- K .

We remark that there is a cheaper procedure to obtain a basis that is equivalent to $\widetilde{\Phi}_{s,\hat{d}}$, whose steps however depend on the expression of $\mathbf{X}_{s,s}$. We first address the case in which $\mathbf{X}_{s,s}$ is rank-1. This is the case when $\mathcal{V} = L^2(\Omega)$, since $\mathbf{X}_{s,s} = \mathbf{M}_{s,s}$ and the mass matrix is indeed rank-1. Secondly, we consider a generic rank- K norm matrix.

In the former scenario, the Cholesky decomposition of a Kronecker product matrix applies:

$$\text{Cholesky}(\mathbf{X}_{1,1} \otimes \cdots \otimes \mathbf{X}_{d,d}) = \mathbf{H}_{1,1} \otimes \cdots \otimes \mathbf{H}_{d,d}. \quad (21)$$

Now, let us recall the diadic representation of $\mathbf{U}_{s,t\mu}$. Let us consider the first unfolding $\mathbf{T}_{1,\gamma_2} = \mathbf{U}_{1,\gamma_2}$. By applying a TSVD with $\varepsilon = 0$, we can write $\mathbf{T}_{1,\gamma_2} = \Phi_{1,\sigma_1} \mathbf{R}_{\sigma_1,\gamma_2}$, where the subindex σ_1 refers to the rank of \mathbf{T}_{1,γ_2} (see Alg. 2 for more details). By applying an SVD on the second unfolding $\mathbf{T}_{\sigma_1,2,\gamma_3} = \mathbf{R}_{\sigma_1,2,\gamma_3}$, we can write $\mathbf{T}_{\sigma_1,2,\gamma_3} = \Phi_{\sigma_1,2,\sigma_2} \mathbf{R}_{\sigma_2,\gamma_3}$. This procedure continues iteratively, until we get

$$\mathbf{U}_{s,t\mu} = \Phi_{1,\sigma_1} \Phi_{\sigma_1,2,\sigma_2} \cdots \Phi_{\sigma_{d-1},d,\sigma_d} \mathbf{R}_{\sigma_d,t\mu}. \quad (22)$$

We refer to [13] for additional details. Now we write the same for $\widetilde{\mathbf{U}}_{s,t\mu}$. Notice that

$$(\mathbf{H}_{1,1} \otimes \cdots \otimes \mathbf{H}_{d,d}) \mathbf{U}_{s,t\mu} = \mathbf{H}_{d,d} (\cdots (\mathbf{H}_{1,1} \mathbf{U}_{1,\dots,d,t\mu})).$$

Now we introduce the rescaled unfolding $\bar{\mathbf{T}}_{1,\gamma_2} = \mathbf{H}_{1,1} \mathbf{T}_{1,\gamma_2}$, which admits a diadic representation $\bar{\mathbf{T}}_{1,\gamma_2} = \bar{\Phi}_{1,\sigma_1} \bar{\mathbf{R}}_{\sigma_1,\gamma_2}$. Then, we rescale the unfolding $\bar{\mathbf{R}}_{\sigma_1,\gamma_2}$ by $\mathbf{H}_{2,2}$, i.e. $\bar{\mathbf{T}}_{\sigma_1,2,\gamma_3} = \mathbf{H}_{2,2} \bar{\mathbf{R}}_{\sigma_1,2,\gamma_3}$, which admits its own diadic format, and so on. By iteration, we can derive a similar expression to (22):

$$(\mathbf{H}_{1,1} \otimes \cdots \otimes \mathbf{H}_{d,d}) \mathbf{U}_{s,t\mu} = \bar{\Phi}_{1,\sigma_1} \bar{\Phi}_{\sigma_1,2,\sigma_2} \cdots \bar{\Phi}_{\sigma_{d-1},d,\sigma_d} \mathbf{R}_{\sigma_d,t\mu}. \quad (23)$$

The representations (22) and (23) admit the same final unfolding $\mathbf{T}_{\sigma_d,t\mu}$, at least in a spectral sense. Note that, if we were to truncate the terms $\bar{\Phi}_{\sigma_{i-1},i,\sigma_i}$ according to the procedure in Alg. 3, the result would not be identical to the cores $\widehat{\Phi}_{i-1,i,\hat{i}}$ identified in Thm. 2. Despite this, ultimately, the subspace $\widetilde{\mathbf{U}}_{s,t\mu}$ spanned by the TT cores $\widehat{\Phi}_{i-1,i,\hat{i}}$ is equal to the subspace $\widetilde{\mathbf{U}}_{s,t\mu}$ spanned by the TT cores $\widetilde{\Phi}_{i-1,i,\hat{i}}$. The only difference between the two approaches is that finding $\widetilde{\Phi}_{i-1,i,\hat{i}}$ is computationally advantageous. This is because we avoid computing the (expensive) Cholesky factorization of $\mathbf{X}_{s,s}$ and the rescaling of the snapshots by $\mathbf{H}_{s,s}$; instead, for every iteration i of the TT-SVD *for* loop, we merely compute $\mathbf{H}_{i,i}$ and rescale the respective unfolding tensor. The number of operations is considerably smaller in this case, since it depends on N_i , rather than the whole number of DOFs N_s as in the previous scenario. This discussion is summarized in Alg. 4.

Algorithm 4 TT-SVD: Given the snapshots tensor in the “split-axes” format \mathbf{U}_{γ_1} , the prescribed accuracy ε , and the 1-d norm matrices $\mathbf{X}_{1,1}, \dots, \mathbf{X}_{d,d}$, build the $\mathbf{X}_{st,st}$ -orthogonal TT-cores $\widehat{\Phi}_{0,1,\widehat{1}}, \dots, \widehat{\Phi}_{d-1,d,\widehat{d}}, \widehat{\Phi}_{\widehat{d},t,\widehat{t}}$

```

1: function TT-SVD( $\mathbf{U}_{\gamma_1}, \mathbf{X}_{i,i}, \varepsilon$ )
2:   Set  $r_0 = 1, \mathbf{T}_{\gamma_1} = \mathbf{U}_{\gamma_1}$ 
3:   for  $i = 1, \dots, d$  do
4:      $i$ th Cholesky factorization:  $\mathbf{H}_{i,i} = \text{Cholesky}(\mathbf{X}_{i,i})$   $\triangleright \mathcal{O}(N_i)$ 
5:      $i$ th spatial rescaling:  $\widetilde{\mathbf{T}}_{i-1,i,\gamma_{i+1}} = \mathbf{H}_{i,i} \mathbf{T}_{i-1,i,\gamma_{i+1}}$   $\triangleright \mathcal{O}(N_{z_i} r_{i-1} N_{\gamma_{i+1}})$ 
6:      $i$ th spatial reduction:  $\widetilde{\Phi}_{i-1,i,\widehat{i}} \widetilde{\mathbf{R}}_{i,\gamma_{i+1}} = \text{TSVD}(\widetilde{\mathbf{T}}_{i-1,i,\gamma_{i+1}})$   $\triangleright \mathcal{O}(\min\{r_{i-1} N_i N_{\gamma_{i+1}}^2, (r_{i-1} N_i)^2 N_{\gamma_{i+1}}\})$ 
7:      $i$ th spatial inverse rescaling:  $\Phi_{i-1,i,\widehat{i}} = \mathbf{H}_{i,i}^{-1} \widetilde{\Phi}_{i-1,i,\widehat{i}}$   $\triangleright \mathcal{O}(N_{z_i} r_{i-1} r_i)$ 
8:     Update unfolding tensor:  $\mathbf{T}_{i,\gamma_{i+1}} = \mathbf{R}_{i,\gamma_{i+1}}$ 
9:   end for
10:  Compute  $\widehat{\Phi}_{\widehat{d},t,\widehat{t}}$  as in Alg. 3  $\triangleright \mathcal{O}(r_d N_t N_\mu^2)$ 
11:  return  $\widehat{\Phi}_{0,1,\widehat{1}}, \dots, \widehat{\Phi}_{d-1,d,\widehat{d}}, \widehat{\Phi}_{\widehat{d},t,\widehat{t}}$ 
12: end function

```

Here, we use N_{z_i} to indicate the nonzero entries of the sparse matrix $\mathbf{X}_{i,i}$. As already observed, the operations concerning the $\mathbf{X}_{s,s}$ -orthogonality are now independent of the global size of the problem N_{st} , as they only scale with the 1-d sizes N_i . The only operation that still depends on N_{st} is the SVD. We briefly discuss the bound of the computational cost of Alg. 4, and we qualitatively compare such bound with the cost of the TPOD. To derive a preliminary bound for Alg. 4, we assume that $N_1 \approx \dots \approx N_d \approx M$. Additionally, we consider a bounding rank r such that $r_i < r$ for every spatial i . Even though the value of r can be very different depending on the problem at hand, our numerical experiments indicate that a bounding rank such that $r = \mathcal{O}(M)$ always exists. We also notice that, within each iteration, the cost is dominated by that of the spatial rescaling and SVD. Thus, neglecting the contributions stemming from the other operations, and given that the cost of the iterations decreases after the first two (this is because γ_i decreases; we cannot neglect the second iteration because r is absent from the first iteration, since $r_0 = 1$), we can bound the cost of Alg. 4 with

$$d \max\{N_2 \cdots N_t (N_z + N_1^2), N_3 \cdots N_t (N_{z_2} + (r_1 N_2)^2)\}.$$

The multiplicative constant d corresponds to the length of the *for* loop. Let us furthermore assume for simplicity that:

- The spatial dimension of the problem is $d = 3$, and that \mathcal{V}_h is a linear FE space. This implies that the number of nonzero entries can be expressed as $N_z \approx 27M^3$, and $N_{z_i} \approx 3M$ for every i .
- N_t and N_μ are such that $N_t \approx N_\mu \approx M$. This assumption is reasonable in many practical applications, as the ones we solve in Sec. 6.

Under these circumstances, the TPOD presented in Alg. 1 has a cost of order

$$\mathcal{O}(M^6 + 27M^5 + 27M^7 + 27r_s M^3 + r_s M^5 + r_s M^3) \sim \mathcal{O}(27M^7).$$

On the other hand, Alg. 4 has a cost of order

$$\mathcal{O}(3 \max\{3M^5 + M^6, 3rN^4 + r^2 M^5\}) \sim \mathcal{O}(3M^5 \max\{M, r^2\}). \quad (24)$$

Our experience suggests that $r^2 > M$, in which case the TT-SVD is cheaper whenever $r < 3M$. Such condition is usually satisfied, as our numerical results demonstrate that TT-SVD is noticeably cheaper than TPOD. This result also suggests that, despite the TT-SVD being potentially (a lot) cheaper, the two methods exhibit a similar behavior in terms of M . In terms of cost, the leading term for both procedures is that of the SVDs. Various algorithms, such as the randomized SVD [27], or the truncated SVD [28] are available to lower the cost of the step. In this work, we opt for a standard SVD algorithm. We also note that when a rigorous *a priori* error bound is not demanded, one may opt for TT-CROSS [13], which employs alternating linear schemes and the CUR approximation to refine an initial TT approximation. This approach updates each individual tensor core, avoiding the need to process the entire snapshots tensor. TT-CROSS is commonly applied in high-dimensional TT approximations [15, 29, 30], though its convergence behavior remains an open problem in current research.

Now, let us consider the more involved case where $\mathbf{X}_{s,s}$ admits the form

$$\mathbf{X}_{s,s} = \sum_{k=1}^K \otimes_{i=1}^d \mathbf{X}_{i,i}^k, \quad (25)$$

with K representing the rank of the norm matrix. This is the case of our FOM, where the norm matrix is given by a stiffness matrix (see (10)). In this scenario, we cannot exploit (21) as we do to derive Alg. 4; let us write the diadic representation of $\mathbf{X}_{s,s} \mathbf{U}_{s,t\mu}$, using the same notation as in (23):

$$\mathbf{X}_{s,s} \mathbf{U}_{s,t\mu} = \sum_{k=1}^K \bar{\mathbf{V}}_{1,\sigma_1^k}^k \bar{\mathbf{V}}_{\sigma_1^k,2,\sigma_2^k}^k \cdots \bar{\mathbf{V}}_{\sigma_{d-1}^k,d,\sigma_d^k}^k \mathbf{T}_{\sigma_d^k,t\mu}^k. \quad (26)$$

Here, $\bar{\mathbf{V}}_{\sigma_i^k, i, \sigma_i^k}^k$ is the i th diadic term, which takes into account the rescaling by $\mathbf{X}_{i,i}^k$. The subscripts σ_i^k now have a superscript k indicating that the rank of the diadic terms might differ across k . The expression (26) motivates the following idea: we consider each of the K addends separately, on which we run independent TT-SVDs. Then, we find a TT decomposition for the sum of the K resulting TT decompositions. To do so, we recall a result from [13].

Proposition 1. *Let us consider two equisized tensors $\mathbf{U}_{\gamma_1}^1, \mathbf{U}_{\gamma_1}^2$ admitting TT decompositions $\{\Phi_{\widehat{i-1}, i, \widehat{i}}^1\}_i$ and $\{\Phi_{\widehat{i^2-1}, i, \widehat{i^2}}^2\}_i$ of ranks $\mathbf{r}^1 = (r_1^1, \dots, r_d^1, r_t^1)$ and $\mathbf{r}^2 = (r_1^2, \dots, r_d^2, r_t^2)$, respectively. Then, their sum $\mathbf{U}_{\gamma_1}^1 + \mathbf{U}_{\gamma_1}^2$ admits the TT decomposition $\{\Phi_{\widehat{i-1}, i, \widehat{i}}\}_i$ of rank $\bar{\mathbf{r}} = \mathbf{r}^1 + \mathbf{r}^2$ such that:*

$$\Phi_{\widehat{0}, 1, \widehat{1}} = \left[\Phi_{\widehat{0}, 1, \widehat{1}}^1, \Phi_{\widehat{0}, 1, \widehat{1}}^2 \right] \in \mathbb{R}^{1 \times N_1 \times r_1^1 + r_1^2}; \quad \Phi_{\widehat{1}, 2, \widehat{2}} = \begin{bmatrix} \Phi_{\widehat{1}, 2, \widehat{2}}^1 & \mathbf{0} \\ \mathbf{0} & \Phi_{\widehat{1}, 2, \widehat{2}}^2 \end{bmatrix} \in \mathbb{R}^{r_1^1 + r_1^2 \times N_2 \times r_2^1 + r_2^2}; \quad \dots \quad (27)$$

We employ the subscript \widehat{i} to indicate the i th summed rank $\bar{r}_i = r_i^1 + r_i^2$. By employing the same notation, we can write the TT approximation of $\mathbf{X}_{s,s} \mathbf{U}_{s,t\mu}$ as

$$\mathbf{X}_{s,s} \mathbf{U}_{s,t\mu} \approx \Phi_{\widehat{0}, 1, \widehat{1}} \cdots \Phi_{\widehat{d-1}, d, \widehat{d}} \mathbf{T}_{d,t\mu} = \Phi_{\widehat{0}, 1, \widehat{1}} \cdots \Phi_{\widehat{d-1}, d, \widehat{d}} \begin{bmatrix} \mathbf{T}_{d^1, t\mu}^1 \\ \vdots \\ \mathbf{T}_{d^K, t\mu}^K \end{bmatrix}. \quad (28)$$

An immediate consequence of (28) is that, even though the spatial subspaces suffer from an increase of dimension, the spatio-temporal TT subspace associated to $\mathbf{X}_{s,s} \mathbf{U}_{s,t\mu}$ still has a dimension of r_t . This was to be expected, since pre-multiplying by $\mathbf{X}_{s,s}$ does not directly affect the temporal evolution of the snapshots. Note, however, that the cores in (28) do not form a hierarchical basis (the concatenation of two or more bases is not necessarily a basis). To remedy this issue, we can run a rank-reducing technique that is reminiscent of a strategy proposed in [13]:

- Compress the first core: $\Phi_{\widehat{1}, \widehat{1}}, \mathbf{R}_{\widehat{1}, \widehat{1}} = \text{TSVD}(\Phi_{\widehat{1}, \widehat{1}})$.
- Rescale the second core: $\Phi_{\widehat{1}, 2, \widehat{2}} = \mathbf{R}_{\widehat{1}, \widehat{1}} \Phi_{\widehat{1}, 2, \widehat{2}}$. Compress the result: $\Phi_{\widehat{1}, 2, \widehat{2}}, \mathbf{R}_{\widehat{2}, \widehat{2}} = \text{TSVD}(\Phi_{\widehat{1}, 2, \widehat{2}})$.
- Continue the procedure until the last axis d .

Since the result of the aforementioned algorithm only satisfies Euclidean orthogonality, we must modify it in order to retrieve an $\mathbf{X}_{s,s}$ -orthogonal decomposition. For this purpose, an efficient algorithm that only runs operations on the cores $\{\Phi_{\widehat{i-1}, i, \widehat{i}}\}_i$ can be derived by writing down the orthogonality condition $\mathbf{I}_{\widehat{s}, \widehat{s}} = \Phi_{\widehat{s}, s} \mathbf{X}_{s,s} \Phi_{\widehat{s}, s}$. For simplicity, we consider the case $d = 2$. Exploiting the Kronecker product property

$$(\mathbf{A} \otimes \mathbf{B})(\mathbf{C} \otimes \mathbf{D}) = (\mathbf{AC}) \otimes (\mathbf{BD}), \quad (29)$$

we have

$$\begin{aligned} \Phi_{\widehat{2}, 1, 2} \mathbf{X}_{12, 12} \Phi_{12, \widehat{2}} &= \sum_{\alpha_1, \alpha_2, \beta_1, \beta_2, k} \left(\Phi_{\widehat{0}, 1, \widehat{1}} [\alpha_0, :, \alpha_1]^T \mathbf{X}_{1,1}^k \Phi_{\widehat{0}, 1, \widehat{1}} [\beta_0, :, \beta_1] \right) \left(\Phi_{\widehat{1}, 2, \widehat{2}} [\alpha_1, :, \alpha_2]^T \mathbf{X}_{2,2}^k \Phi_{\widehat{1}, 2, \widehat{2}} [\beta_1, :, \beta_2] \right) \\ &= \sum_{\alpha_2, \beta_2} \sum_{\alpha_1, \beta_1} \Phi_{\widehat{1}, 2, \widehat{2}} [\alpha_1, :, \alpha_2] \left(\sum_k \widehat{\mathbf{X}}_{\widehat{1}, \widehat{1}}^k [\alpha_1, \beta_1] \mathbf{X}_{2,2}^k \right) \Phi_{\widehat{1}, 2, \widehat{2}} [\beta_1, :, \beta_2] \\ &= \Phi_{\widehat{2}, \widehat{1}, 2} \widehat{\mathbf{X}}_{\widehat{1}, \widehat{1}} \Phi_{\widehat{1}, 2, \widehat{2}}. \end{aligned} \quad (30)$$

The matrices $\widehat{\mathbf{X}}_{\widehat{1}, \widehat{1}}^k$ and $\widehat{\mathbf{X}}_{\widehat{1}, \widehat{1}, 2}$ are given by

$$\widehat{\mathbf{X}}_{\widehat{1}, \widehat{1}}^k [\alpha_1, \beta_1] = \Phi_{\widehat{0}, 1, \widehat{1}} [\alpha_0, :, \alpha_1]^T \mathbf{X}_{1,1}^k \Phi_{\widehat{0}, 1, \widehat{1}} [\beta_0, :, \beta_1], \quad \widehat{\mathbf{X}}_{\widehat{1}, \widehat{1}, 2} = \sum_{k=1}^K \mathbf{X}_{2,2}^k \otimes \widehat{\mathbf{X}}_{\widehat{1}, \widehat{1}}^k.$$

Eq. (30) tells us that requiring $\mathbf{X}_{12, 12}$ -orthogonality of the spatial basis $\Phi_{12, \widehat{2}}$ is equivalent to enforcing the $\widehat{\mathbf{X}}_{\widehat{1}, \widehat{1}, 2}$ -orthogonality of $\Phi_{\widehat{1}, 2, \widehat{2}}$. Note that the modified norm matrix $\widehat{\mathbf{X}}_{\widehat{1}, \widehat{1}, 2}$ is sparse, with a number of elements equal to $r_1^2 N_{z_2}$. Generalizing to the case of an arbitrary $d \geq 2$, we require $\Phi_{\widehat{d-1}, d, \widehat{d}}$ to be orthogonal with respect to

$$\widehat{\mathbf{X}}_{\widehat{d-1}, d, \widehat{d-1}} = \sum_{k=1}^K \mathbf{X}_{d,d}^k \otimes \widehat{\mathbf{X}}_{\widehat{d-1}, \widehat{d-1}}^k, \quad (31)$$

where

$$\widehat{\mathbf{X}}_{\widehat{i}, \widehat{i}}^k [\alpha_i, \beta_i] = \widehat{\mathbf{X}}_{\widehat{i-1}, \widehat{i-1}}^k [\alpha_{i-1}, \beta_{i-1}] \Phi_{\widehat{i-1}, i, \widehat{i}} [\alpha_{i-1}, :, \alpha_i]^T \mathbf{X}_{i,i}^k \Phi_{\widehat{i-1}, i, \widehat{i}} [\beta_{i-1}, :, \beta_i]. \quad (32)$$

Notice that the relationship (32) is recursive, and therefore the final matrix (31) can be built iteratively. The entire procedure that produces an $\mathbf{X}_{st, st}$ -orthogonal basis, where the (spatial) norm matrix admits the form (25), is summarized in Alg. 5. We note that the orthogonalization procedure has only a marginal impact on the overall cost of the algorithm, which still largely scales with the SVD calls. Therefore, a similar estimate to (24) holds. The only difference is given by

the multiplicative constant, which we recall is simply the length of the *for* loop. Such length is now given by Kd , whereas previously it was merely d . If we consider the norm matrix (10), we have $K = d = 3$, and thus the complexity is of order $\mathcal{O}(9M^5 \max\{M, r^2\})$.

Algorithm 5 TT-SVD: Given the snapshots tensor in the “split-axes” format U_{γ_1} , the prescribed accuracy ε , and the 1-d norm matrices $X_{1,1}^k, \dots, X_{d,d}^k$ for every k , build the $X_{st,st}$ -orthogonal TT-cores $\Phi_{0,1,\hat{1}}, \dots, \Phi_{\widehat{d-1},d,\widehat{d}}, \Phi_{\widehat{d},t,\widehat{t}}$.

```

1: function TT-SVD( $U_{\gamma_1}, X_{i,i}^k, \varepsilon$ )
2:   Set  $r_0^k = 1, T_{\gamma_1}^k = U_{\gamma_1}$  for every  $k$ 
3:   Initialize rescaling matrix:  $R_{\widehat{0},\widehat{0}} = [1] \in \mathbb{R}^{1 \times 1}$ 
4:   Initialize weight matrix  $\widehat{X}_{\widehat{0},\widehat{0}}^k = [1] \in \mathbb{R}^{1 \times 1}$  for every  $k$ 
5:   for  $i = 1, \dots, d$  do
6:     for  $k = 1, \dots, K$  do
7:       Compute  $\Phi_{i^{k-1},i,\widehat{i}^k}$ , update  $T_{\widehat{i}^k,\gamma_{i+1}}^k$  as in Alg. 4  $\triangleright \mathcal{O}\left(\min\{r_{i-1}^k N_i N_{\gamma_{i+1}}^2, (r_{i-1}^k N_i)^2 N_{\gamma_{i+1}}\}\right)$ 
8:     end for
9:     Define  $\Phi_{i-1,i,\widehat{i}}$  as in (27)
10:     $i$ th rescaling:  $\Phi_{i-1,i,\widehat{i}} = R_{i-1,i-1} \Phi_{i-1,i,\widehat{i}}$   $\triangleright \mathcal{O}(N_i r_{i-1} \bar{r}_{i-1} \bar{r}_i)$ 
11:    if  $i < d$  then
12:       $i$ th rank reduction, update rescaling matrix:  $\Phi_{i-1,i,\widehat{i}}, R_{i,\widehat{i}} = \text{TSVD}(\Phi_{i-1,i,\widehat{i}}, \varepsilon)$   $\triangleright \mathcal{O}(r_{i-1} N_i \bar{r}_i^2)$ 
13:      for  $k = 1, \dots, K$  do
14:        Update weight matrix  $\widehat{X}_{i,\widehat{i}}^k$  as in (32)  $\triangleright \mathcal{O}(N_{z_i} r_{i-1}^k r_i^k + N_i (r_{i-1}^k r_i^k)^2 + (r_{i-1}^k r_i^k)^2)$ 
15:      end for
16:      else if  $i = d$  then
17:        Compute final weight  $\widehat{X}_{d-1,d,\widehat{d-1}}$  as in (31)  $\triangleright \mathcal{O}(K N_{z_d} r_{d-1}^2)$ 
18:        Cholesky factorization:  $\widehat{H}_{d-1,d,\widehat{d-1}} = \text{Cholesky}(\widehat{X}_{d-1,d,\widehat{d-1}})$   $\triangleright \mathcal{O}(r_{d-1}^2 N_d)$ 
19:         $d$ th rank reduction:  $\Phi_{d-1,d,\widehat{d}}, R_{d,\widehat{d}} = \text{TSVD}(\widehat{H}_{d-1,d,\widehat{d-1}} \Phi_{d-1,d,\widehat{d}}, \varepsilon)$   $\triangleright \mathcal{O}(r_{d-1} N_d \bar{r}_d^2)$ 
20:        Inverse rescaling:  $\Phi_{d-1,d,\widehat{d}} = \widehat{H}_{d-1,d,\widehat{d-1}}^{-1} \Phi_{d-1,d,\widehat{d}}$   $\triangleright \mathcal{O}(N_{z_d} r_{d-1}^2 r_d)$ 
21:      end if
22:    end for
23:    Compute  $\Phi_{\widehat{d},t,\widehat{t}}$  as in Alg. 3  $\triangleright \mathcal{O}(r_d N_t N_\mu^2)$ 
24:    return  $\Phi_{0,1,\widehat{1}}, \dots, \Phi_{\widehat{d-1},d,\widehat{d}}, \Phi_{\widehat{d},t,\widehat{t}}$ 
25: end function

```

4.2. Empirical interpolation method. Let us consider the reduced linear system (12). Since the LHS and RHS are parameter-dependent, they must in principle be computed during the online phase for any new choice of μ . A more feasible ROM consists in firstly finding an affine approximant of these quantities, featuring a parameter-independent basis and a parameter-dependent reduced coefficient, as shown in (13), and secondly, solving the affine counterpart (14). A collocation method, e.g., an empirical interpolation method (EIM), is typically employed for this task. Among the most well-known EIMs, we mention the discrete empirical interpolation method (DEIM) [31], and its matrix version MDEIM [32]. We recall in Alg. 6 the procedure for a space-time MDEIM, as presented in [3] (the symbol $e_s(i)$ indicates the i th vector of the N_s -dimensional canonical basis). This procedure is computationally demanding because of the TPOD we run to compute $\Phi_{s,\widehat{s}}^L$ and $\Phi_{t,\widehat{t}}^L$, but it can be run offline. After running Alg. 6, given an online parameter $\mu \in \mathcal{D}_{\text{on}}$, we empirically interpolate L_{st}^μ as

$$L_{st}^\mu \approx \widehat{L}_{st}^\mu = \left(\Phi_{s,\widehat{s}}^L \otimes \Phi_{t,\widehat{t}}^L \right) \widehat{L}_{st}^\mu, \quad \text{where} \quad \widehat{L}_{st}^\mu = \left(P_{\widehat{s},s}^L \Phi_{s,\widehat{s}}^L \otimes P_{\widehat{t},t}^L \Phi_{t,\widehat{t}}^L \right)^{-1} \left(P_{\widehat{s},s}^L \otimes P_{\widehat{t},t}^L \right) L_{st}^\mu. \quad (33)$$

We recall the accuracy of the Alg. 6:

$$\left\| L_{st}^\mu - \widehat{L}_{st}^\mu \right\|_2 \leq \varepsilon \left\| \left(P_{\widehat{s},s}^L \Phi_{s,\widehat{s}}^L \otimes P_{\widehat{t},t}^L \Phi_{t,\widehat{t}}^L \right)^{-1} \right\|_F \sqrt{\|L_{s,t,\mu}\|_F^2 + \|\widehat{L}_{t,\widehat{s},\mu}\|_F^2}.$$

We refer to [3] for a complete proof of the statement. In TT-RB, we change the first line of Alg. 6 with a call to a standard TT-SVD, as presented in Alg. 3 (since we simply require an Euclidean orthogonality for the residual basis). In this scenario, we seek an approximation in the form

$$L_{st}^\mu \approx \widehat{L}_{st}^\mu = \left(\Phi_{0,1,\widehat{1}}^L \cdots \Phi_{\widehat{d},t,\widehat{t}}^L \right) \widehat{L}_{\widehat{t}}^\mu,$$

where

$$\widehat{L}_{\widehat{t}}^\mu = \left(P_{\widehat{t},st}^L \left(\Phi_{0,1,\widehat{1}}^L \cdots \Phi_{\widehat{d},t,\widehat{t}}^L \right) \right)^{-1} P_{\widehat{t},st}^L L_{st}^\mu = \left(P_{\widehat{t},st}^L \Phi_{st,\widehat{t}}^L \right)^{-1} P_{\widehat{t},st}^L L_{st}^\mu. \quad (34)$$

Algorithm 6 ST-MDEIM: Given the tensor of space-time residual snapshots $\mathbf{L}_{s,t,\mu}$ and the prescribed accuracy ε , build the ℓ^2 -orthogonal bases $\Phi_{s,\hat{s}}^L$, $\Phi_{t,\hat{t}}^L$, and sampling matrices $\mathbf{P}_{s,\hat{s}}^L \in \{0, 1\}^{N_s \times n_s^L}$, $\mathbf{P}_{t,\hat{t}}^L \in \{0, 1\}^{N_t \times n_t^L}$.

```

1: function ST-MDEIM( $\mathbf{L}_{s,t,\mu}, \varepsilon$ )
2:   Compute  $\Phi_{s,\hat{s}}^L, \Phi_{t,\hat{t}}^L = \text{TPOD}(\mathbf{L}_{s,t,\mu}, \varepsilon)$  as in Alg. 1
3:   Set  $\mathbf{P}_{s,\hat{s}}^L = [\mathbf{e}_s(i^1)]$ , where  $i^1 = \arg \max |\Phi_{s,\hat{s}}^L[:, 1]|$ 
4:   for  $q \in \{2, \dots, n_s^L\}$  do
5:     Set  $\mathbf{V}_s = \Phi_{s,\hat{s}}^L[:, q]$ ,  $\mathbf{V}_{s,\hat{s}} = \Phi_{s,\hat{s}}^L[:, 1 : q - 1]$ 
6:     Compute residual  $\mathbf{r}_s = \mathbf{V}_s - \mathbf{V}_{s,\hat{s}} \left( \mathbf{P}_{s,\hat{s}}^L \mathbf{V}_{s,\hat{s}} \right)^{-1} \mathbf{P}_{s,\hat{s}}^L \mathbf{V}_s$ 
7:     Update  $\mathbf{P}_{s,\hat{s}}^L = [\mathbf{P}_{s,\hat{s}}^L, \mathbf{e}_s(i^q)]$ , where  $i^q = \arg \max |\mathbf{r}_s|$ 
8:   end for
9:   Compute  $\mathbf{P}_{t,\hat{t}}^L$  in the same way
10:  return  $\Phi_{s,\hat{s}}^L, \Phi_{t,\hat{t}}^L, \mathbf{P}_{s,\hat{s}}^L, \mathbf{P}_{t,\hat{t}}^L$ 
11: end function

```

Here, $\{\Phi_{i-1,i,\hat{i}}^L\}_i$ indicates the TT decomposition of the residual, of ranks r_1^L, \dots, r_t^L . Even though the ranks differ from the ones computed from the snapshots U_{γ_1} , for simplicity, we employ the same reduced subindices \hat{i} in both cases. We only use the subindex \hat{i}^L when this notation may be ambiguous. Upon computing the TT cores $\Phi_{i-1,i,\hat{i}}^L$ for every i , we seek the matrix of interpolation indices $\mathbf{P}_{st,\hat{t}}^L$. For this purpose, one could follow a naive approach, which consists in computing the space-time basis $\Phi_{st,\hat{t}}^L$ from the residual cores (see (15)), and then run the *for* loop in Alg. 6. However, the direct assembly of $\Phi_{st,\hat{t}}^L$ requires a considerable number of operations, and thus should be avoided. Alternatively, we must tweak the *for* loop to account for the fact that we are not dealing with a basis in matrix form, rather a sequence of cores. To this end, we propose TT-MDEIM, which exploits the hierarchical structure of TT decompositions to compute the desired matrix of indices by performing only operations on the cores. This procedure comprises an initial left-to-right swipe on the TT cores, whereupon the intermediate interpolation matrices $\tilde{\mathbf{P}}_{i-1,i,\hat{i}}^L$ are returned; and a subsequent right-to-left swipe on said intermediate interpolation matrices to recover the entire interpolation matrix $\mathbf{P}_{st,\hat{t}}^L$. The two steps are represented graphically in Figs. 2-3. Even though TT-MDEIM computes an interpolation matrix that is not equivalent to that obtained with the naive approach, we show in Thm. 3 that the two methods exhibit the same accuracy with respect to ε . TT-MDEIM draws inspiration from [33], where the authors propose a method combining DEIM and TT-CROSS to compute the TT decomposition of a tensor, and from [34], where an algorithm for the search of the maximum absolute value in a TT decomposition is discussed. We give a qualitative explanation on how TT-MDEIM is implemented, in the case $d = 2$. For simplicity, we denote as EIM-LOOP the function consisting of the *for* loop in Alg. 6, which returns an interpolation matrix from a given basis.

The first step of the procedure consists of a left-to-right swipe of the TT cores to compute the intermediate matrices $\tilde{\mathbf{P}}_{i-1,i,\hat{i}}^L$:

- We compute the first matrix of indices: $\tilde{\mathbf{P}}_{1,\hat{1}}^L = \text{EIM-LOOP}(\tilde{\Phi}_{1,\hat{1}}^L)$, where $\tilde{\Phi}_{1,\hat{1}}^L = \Phi_{1,\hat{1}}^L$.
- We restrict the first core to the indices in $\tilde{\mathbf{P}}_{1,\hat{1}}^L$: $\tilde{\Phi}_{1,\hat{1}}^L = \tilde{\mathbf{P}}_{1,\hat{1}}^L \Phi_{1,\hat{1}}^L$.
- We compute the $r_1 N_2$ -dimensional subspace $\tilde{\Phi}_{12,\hat{2}}^L = \tilde{\Phi}_{1,\hat{1}}^L \Phi_{1,2,\hat{2}}^L$, and we find $\tilde{\mathbf{P}}_{12,\hat{2}}^L = \text{EIM-LOOP}(\tilde{\Phi}_{12,\hat{2}}^L)$.
- We repeat: compute (1) $\tilde{\Phi}_{2,\hat{2}}^L = \tilde{\mathbf{P}}_{12,\hat{2}}^L \tilde{\Phi}_{12,\hat{2}}^L$, (2) $\tilde{\Phi}_{2t,\hat{t}}^L = \tilde{\Phi}_{2,\hat{2}}^L \Phi_{2,t,\hat{t}}^L$, and (3) $\tilde{\mathbf{P}}_{2t,\hat{t}}^L = \text{EIM-LOOP}(\tilde{\Phi}_{2t,\hat{t}}^L)$.

Next, we aim to compute the final interpolation matrix $\mathbf{P}_{st,\hat{t}}^L$ from the intermediate ones. To this end, we introduce the index mapping \mathcal{K} for a Kronecker product:

$$\mathbf{A}[\mathcal{K}(i_1, i_d), \mathcal{K}(j_1, j_2)] = \mathbf{A}_1[i_1, j_1] \otimes \mathbf{A}_2[i_2, j_2], \quad \text{where } \mathbf{A} = \mathbf{A}_1 \otimes \mathbf{A}_2. \quad (35)$$

Naturally, the expression of \mathcal{K} depends on the size of the factors \mathbf{A}_1 and \mathbf{A}_2 . However, for simplicity of notation, we omit this dependence when referring to \mathcal{K} . Let us now consider the last temporary matrix $\tilde{\mathbf{P}}_{2t,\hat{t}}^L$. Each of its r_t columns encodes a row index belonging to $\mathbb{N}(r_2 N_t)$, where we recall that $\mathbb{N}(k) = \{1, \dots, k\}$ for any integer k . By applying the inverse of \mathcal{K} (which is a bijective map, so the inverse is well defined) on the row index, we obtain a tuple of row indices, belonging to $\mathbb{N}(r_2)$ and $\mathbb{N}(N_t)$ respectively. We can repeat this operation for every column of $\tilde{\mathbf{P}}_{2t,\hat{t}}^L$. With a slight abuse of notation, we refer to this process as

$$\left(\tilde{\mathbf{P}}_{2,\hat{t}}^L, \mathbf{P}_{t,\hat{t}}^L \right) = \mathcal{K}^{-1}(\tilde{\mathbf{P}}_{2t,\hat{t}}^L) \quad (36)$$

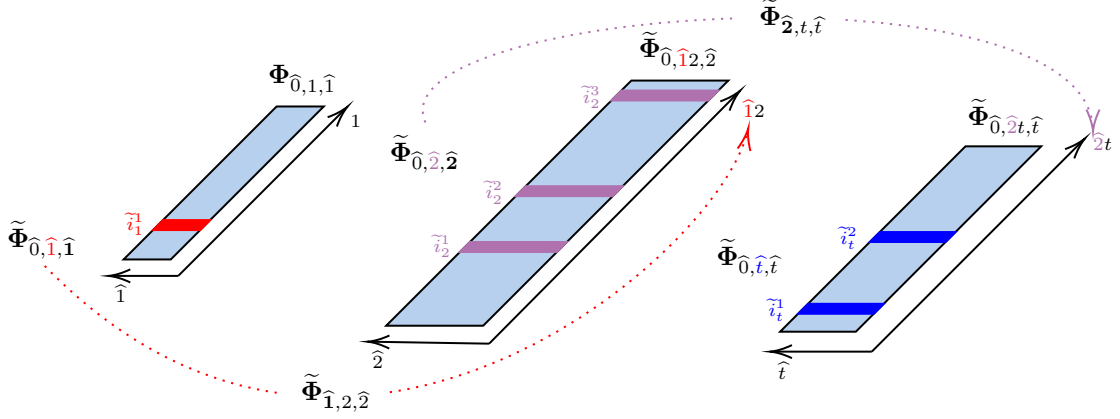


FIGURE 2. Forward swipe on the cores, TT-MDEIM.

The operation in (36) returns a matrix $\mathbf{P}_{t,\hat{t}}^L$ which encodes the MDEIM rows on the temporal axis, and another intermediate matrix $\tilde{\mathbf{P}}_{2,\hat{t}}^L$. The idea of the backward swipe is to propagate the process backwards until every temporary matrix is decomposed according to (36). In summary:

- Exploiting (36), we split $(\tilde{\mathbf{P}}_{2,\hat{t}}^L, \mathbf{P}_{t,\hat{t}}^L) = \mathcal{K}^{-1}(\tilde{\mathbf{P}}_{2t,\hat{t}}^L)$.
- We compute $\tilde{\mathbf{P}}_{12,\hat{t}}^L = \tilde{\mathbf{P}}_{12,2}^L \tilde{\mathbf{P}}_{2,\hat{t}}^L$, and as before we split $(\tilde{\mathbf{P}}_{1,\hat{t}}^L, \mathbf{P}_{2,\hat{t}}^L) = \mathcal{K}^{-1}(\tilde{\mathbf{P}}_{12,\hat{t}}^L)$.
- We compute $\tilde{\mathbf{P}}_{1,\hat{t}}^L = \tilde{\mathbf{P}}_{1,1}^L \tilde{\mathbf{P}}_{1,\hat{t}}^L$, and we set $\mathbf{P}_{1,\hat{t}}^L = \tilde{\mathbf{P}}_{1,\hat{t}}^L$.

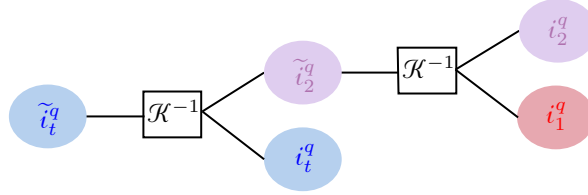


FIGURE 3. Backward swipe on the temporary indices, TT-MDEIM.

Applying the mapping \mathcal{K} on the final matrices $\mathbf{P}_{1,\hat{t}}$, $\mathbf{P}_{2,\hat{t}}$, and $\mathbf{P}_{t,\hat{t}}$ yields the target interpolation matrix $\mathbf{P}_{st,\hat{t}}$. With another abuse of notation, we can indicate this operation as

$$\mathbf{P}_{st,\hat{t}} = \mathcal{K} \left(\mathcal{K} \left(\mathbf{P}_{1,\hat{t}}, \mathbf{P}_{2,\hat{t}} \right), \mathbf{P}_{t,\hat{t}} \right).$$

Remark 1. The procedure above returns not only the interpolation matrix $\mathbf{P}_{st,\hat{t}}^L$, but also the quantity $\mathbf{P}_{t,st}^L \Phi_{st,\hat{t}}^L$, which is needed in the TT-MDEIM approximation, as shown in (34). In fact, we have that

$$\mathbf{P}_{t,st}^L \Phi_{st,\hat{t}}^L = \tilde{\mathbf{P}}_{t,2t}^L \tilde{\Phi}_{2t,\hat{t}}^L.$$

We recall that both $\tilde{\mathbf{P}}_{2t,\hat{t}}^L$ and $\tilde{\Phi}_{2t,\hat{t}}^L$ are computed during the last step in the forward swipe. Instead of providing a rigorous proof, we refer to Fig. 2, which provides an illustration of this statement.

We refer to [33] for a discussion on the computational cost of the method. Here we omit it, as it is in any case negligible with respect to the cost of computing the TT decomposition of the residual. We present in the following theorem the accuracy of TT-MDEIM.

Theorem 3. Let $\mathbf{P}_{st,\hat{t}}^L$ be computed by applying the procedure above on $\Phi_{st,\hat{t}}^L$. The following equation holds:

$$\left\| \mathbf{L}_{st}^\mu - \hat{\mathbf{L}}_{st}^\mu \right\|_2 \leq \varepsilon \sqrt{d+1} \chi^L \left\| \mathbf{L}_{st,\mu} \right\|_F; \quad \chi^L = \left\| \left(\tilde{\mathbf{P}}_{t,2t}^L \tilde{\Phi}_{2t,\hat{t}}^L \right)^{-1} \right\|_F. \quad (37)$$

Proof. Firstly, note that the matrices $\tilde{\Phi}_{1,\hat{t}}^L, \dots, \tilde{\Phi}_{d,\hat{t}}^L, \tilde{\Phi}_{t,\hat{t}}^L$ are full rank (see [33], Lemma 2.1). Thus, Lemma 3.2 in [31] applies:

$$\left\| \mathbf{L}_{st}^\mu - \hat{\mathbf{L}}_{st}^\mu \right\|_2 \leq \left\| \left(\mathbf{P}_{t,st}^L \Phi_{st,\hat{t}}^L \right)^{-1} \right\|_F \left\| \left(\mathbf{I}_{st,st} - \Phi_{st,t}^L \Phi_{t,st}^L \right) \mathbf{L}_{st,\mu} \right\|_F = \chi^L \left\| \left(\mathbf{I}_{st,st} - \Phi_{st,t}^L \Phi_{t,st}^L \right) \mathbf{L}_{st,\mu} \right\|_F.$$

The equality above was derived using Remark 1. Invoking Thm. 1, we have that

$$\left\| \left(\mathbf{I}_{st,st} - \Phi_{st,\hat{t}}^L \Phi_{\hat{t},st}^L \right) \mathbf{L}_{st,\mu} \right\|_F \leq \varepsilon \sqrt{d+1} \|\mathbf{L}_{st,\mu}\|_F,$$

which proves the statement (37) of the theorem. \square

Notice that the accuracy estimate (37) is exactly the same one we would obtain if we naively decided to first assemble $\Phi_{st,\hat{t}}$, and then run the *for* loop in Alg. 6. The only difference is that naive method returns a selection of indices that explicitly minimizes the error due to interpolation χ^L , whereas the indices selected by TT-MDEIM might differ from the former. However, our numerical results show not only that the difference in χ^L is negligible, but it is in fact machine precision, thus suggesting that TT-MDEIM achieves the same accuracy as MDEIM.

4.3. Approximation of the Jacobians. In order to implement the TT-MDEIM for the approximation of the space-time Jacobians, we need to first implement a “split axes” format for these quantities. We assume for simplicity that the sparsity pattern of the Jacobians does not vary for different values of μ . Let us momentarily consider a steady-state Jacobian $\mathbf{K}_{s,s}^\mu$. Since we operate on a Cartesian geometry, it is possible to define an index mapping

$$\mathcal{J}_z : \mathbb{N}(N_{z_1}) \times \cdots \times \mathbb{N}(N_{z_d}) \longrightarrow \mathbb{N}(N_z) \quad (38)$$

that associates an index corresponding to a nonzero entry of $\mathbf{K}_{s,s}^\mu$ to a tuple of indices corresponding to the nonzero entries of $\mathbf{K}_{1,1}^\mu, \dots, \mathbf{K}_{d,d}^\mu$. Note that, in general, there is no direct relationship between the entries of $\mathbf{K}_{s,s}^\mu$ and those of $\mathbf{K}_{1,1}^\mu, \dots, \mathbf{K}_{d,d}^\mu$, in the sense that usually $\mathbf{K}_{1,1}^\mu \otimes \cdots \otimes \mathbf{K}_{d,d}^\mu \neq \mathbf{K}_{s,s}^\mu$. However, it is still possible to recover information related to the sparsity of the Jacobian from the sparsities of $\mathbf{K}_{1,1}^\mu, \dots, \mathbf{K}_{d,d}^\mu$. The mapping (38) allows us to identify the following “split-axes” formulation for the steady state Jacobian, or equivalently its vector of nonzeros \mathbf{K}_z^μ :

$$\mathbf{K}_{z_1, \dots, z_d}^\mu [i_{z_1}, \dots, i_{z_d}] = \mathbf{K}_z^\mu [i_z], \quad \mathcal{J}_z(i_{z_1}, \dots, i_{z_d}) = i_z.$$

Given our assumption of fixed sparsity across the parameters, we can use the mapping (38) to interchangeably consider the snapshots tensors $\mathbf{K}_{s,s,\mu}$, $\mathbf{K}_{z,\mu}$ and $\mathbf{K}_{z_1, \dots, z_d, \mu}$. Similarly, in unsteady applications we have the congruence by isometry relationships

$$\mathbf{K}_{st,st,\mu} \cong \mathbf{K}_{z,t,\mu} \cong \mathbf{K}_{z_1, \dots, z_d, t, \mu}.$$

Running Alg. 3 on $\mathbf{K}_{z_1, \dots, z_d, t, \mu}$ yields the TT decomposition

$$\{\Phi_{0,z_1,\hat{1}}^K, \dots, \Phi_{d-1,z_d,\hat{d}}^K, \Phi_{\hat{d},t,\hat{t}}^K\}.$$

As a consequence, we can run the following TT-MDEIM approximation for the Jacobians:

$$\mathbf{K}_{zt}^\mu \approx \widehat{\mathbf{K}}_{zt}^\mu = \left(\Phi_{0,z_1,\hat{1}}^K \cdots \Phi_{\hat{d},t,\hat{t}}^K \right) \widehat{\mathbf{K}}_{\hat{t}}^\mu, \quad (39)$$

where

$$\widehat{\mathbf{K}}_{\hat{t}}^\mu = \left(\mathbf{P}_{\hat{t},zt}^K \left(\Phi_{0,z_1,\hat{1}}^K \cdots \Phi_{\hat{d},t,\hat{t}}^K \right) \right)^{-1} \mathbf{P}_{\hat{t},zt}^K \mathbf{K}_{zt}^\mu = \left(\mathbf{P}_{\hat{t},zt}^K \Phi_{zt,\hat{t}}^K \right)^{-1} \mathbf{P}_{\hat{t},zt}^K \mathbf{K}_{zt}^\mu.$$

We lastly remark that, by exploiting the sparsity of $\mathbf{K}_{i,i}^\mu$, the spatial cores can equivalently be represented as 4-d sparse arrays:

$$\Phi_{i-1,i,i,\hat{i}}^K \cong \Phi_{i-1,z_i,\hat{i}}^K. \quad (40)$$

We exploit the congruence (40) in the following subsection, when detailing the Galerkin projection of (39) onto the TT-RB subspace identified by (15).

4.4. Galerkin projection. In this subsection, we describe how we assemble the reduced problem (14) when employing the TT-RB method. In this case, the projection operator is given by (15), and the residuals and Jacobians are approximated via TT-MDEIM. The assembly requires the Galerkin projection of the TT-MDEIM approximations on the TT-RB subspace. As we have done in the previous subsections, we commence by recalling the procedure in a standard ST-RB setting. Additionally, we only describe the procedure behind the Galerkin projection of the Jacobian, which is more intricate than that of the residual. Recalling the definition of \mathcal{K} in (35), the Jacobian projection in a standard ST-RB method requires computing

$$\begin{aligned} \widehat{\mathbf{K}}_{\hat{s}\hat{t},\hat{s}\hat{t}}^\mu &= \left(\Phi_{\hat{s},s} \otimes \Phi_{\hat{t},t} \right) \left(\sum_{i_s=1}^{r_s^K} \sum_{i_t=1}^{r_t^K} \left(\Phi_{s,\hat{s}\mathcal{K},s}^K [:, i_s, :] \otimes \Phi_{t,\hat{t}\mathcal{K}}^K [:, i_t] \right) \widehat{\mathbf{K}}_{\hat{s}\hat{t}\mathcal{K}}^\mu [\mathcal{K}(i_s, i_t)] \right) \left(\Phi_{s,\hat{s}} \otimes \Phi_{t,\hat{t}} \right) \\ &= \sum_{i_s=1}^{r_s^K} \sum_{i_t=1}^{r_t^K} \left(\left(\Phi_{\hat{s},s} \Phi_{s,\hat{s}\mathcal{K},s}^K [:, i_s, :] \Phi_{s,\hat{s}} \right) \otimes \widehat{\Phi}_{\hat{t},\hat{t}\mathcal{K},\hat{t}}^K [:, i_t, :] \right) \widehat{\mathbf{K}}_{\hat{s}\hat{t}\mathcal{K}}^\mu [\mathcal{K}(i_s, i_t)], \end{aligned} \quad (41)$$

where we have introduced

$$\widehat{\Phi}_{\hat{t},\hat{t}\mathcal{K},\hat{t}}^K \in \mathbb{R}^{n_t \times n_t^K \times n_t}, \quad \widehat{\Phi}_{\hat{t},\hat{t}\mathcal{K},\hat{t}}^K[\alpha, i_t, \beta] = \sum_{n=1}^{N_t} \Phi_{t,\hat{t}}^K[n, \alpha] \Phi_{t,\hat{t}\mathcal{K}}^K[n, i_t] \Phi_{t,\hat{t}}^K[n, \beta].$$

As shown above, the Jacobian reduction comprises a Kronecker product of a spatial and a temporal factor, the result of which is multiplied by the μ -dependent coefficient. The former operation is run offline, while the latter occurs during the online phase. The cost of the reduction is dominated by the computation of the spatial factor (since $N_z \gg N_t$ in practical applications, the cost of the temporal factor is negligible). Making the same assumptions as in Subsection 4.1, i.e. $N_z \approx 27M^3$, the cost of (41) scales as $\mathcal{O}(27r_{st}^K r_s^2 M^3)$.

Let us now consider the Jacobian compression in a TT framework. Exploiting the property (29) and skipping some computations that are conceptually straightforward but of tedious notation, we can write the Galerkin projection as

$$\begin{aligned} \widehat{\mathbf{K}}_{\hat{t},\hat{t}}^\mu &= \sum_{\alpha_1,\beta_1,\delta_1} \Phi_{\hat{0},1,\hat{1}}[\alpha_0, :, \alpha_1]^T \Phi_{\hat{0}^K,1,1,\hat{1}^K}[\beta_0, :, :, \beta_1] \Phi_{\hat{0},1,\hat{1}}[\delta_0, :, \delta_1] \cdot \\ &\quad \sum_{\alpha_2,\beta_2,\delta_2} \cdots \sum_{\alpha_d,\beta_d,\delta_d} \Phi_{\hat{d-1},d,\hat{d}}[\alpha_{d-1}, :, \alpha_d]^T \Phi_{\hat{d-1}^K,d,d,\hat{d}^K}[\beta_{d-1}, :, :, \beta_d] \Phi_{\hat{d-1},d,\hat{d}}[\delta_{d-1}, :, \delta_d] \cdot \\ &\quad \sum_{\beta_t} \sum_{n=1}^{N_t} \Phi_{\hat{d},t,\hat{t}}[\alpha_d, n, :]^T \Phi_{\hat{d}^K,t,t,\hat{t}^K}[\beta_d, n, \beta_t] \Phi_{\hat{d},t,\hat{t}}[\delta_d, n, :] \widehat{\mathbf{K}}_{\hat{t}^K}^\mu[\beta_t] \\ &= \widehat{\Phi}_{\hat{t},\hat{t}^K}^K \widehat{\mathbf{K}}_{\hat{t}^K}^\mu \end{aligned} \quad (42)$$

Despite the presence of many indices, the computations in (42) expresses in terms of multiple 3d and 4-d TT cores the same spatial and temporal compressions already discussed in (41) for the ST-RB. Making the same assumptions as in Subsection 4.1, and additionally $r_i^K < r^K$ for every i , it is possible to show that the cost scales with $\mathcal{O}(10M(r^2 r^K)^2)$. In our experience, this estimate can be greater than that in the ST-RB case; however, we note that the Galerkin projection is usually far cheaper than the computation of the basis for the Jacobian, therefore making this difference irrelevant.

4.5. Accuracy. In this subsection we state the accuracy of the TT-RB method. The result is a simple application of what is already presented in [3], in the case of the standard ST-RB. Before beginning, we must first introduce some preliminary quantities.

- The coercivity constant, in the $\mathbf{X}_{st,st}$ -norm, of the full order Jacobian:

$$C = \inf_{\mathbf{V}_{st}} \frac{\|\mathbf{K}_{st,st}^\mu \mathbf{V}_{st}\|_{\mathbf{X}_{st,st}^{-1}}}{\|\mathbf{V}_{st}\|_{\mathbf{X}_{st,st}}} = \left\| \mathbf{X}_{st,st}^{-1/2} \mathbf{K}_{st,st}^\mu \mathbf{X}_{st,st}^{-1/2} \right\|_2.$$

- The TT-MDEIM error due to interpolation χ^K and χ^L , for the Jacobian and the residual respectively (see (37)).

We can write the error committed by TT-RB as the sum of two contributions, as in [3, 32]. The first is associated to the TT-MDEIM hyper-reduction. The second stems from the Galerkin projection onto the subspace spanned by $\Phi_{st,\hat{t}}$.

Theorem 4. *Let us consider the well-posed problem given by (9), and its approximation in (14) obtained by combining the TT-SVD and TT-MDEIM algorithms. Denoting the FOM solution as \mathbf{U}_{st}^μ and its approximation as $\widehat{\mathbf{U}}_{st}^\mu$, the following approximation holds:*

$$\begin{aligned} \left\| \mathbf{U}_{st}^\mu - \widehat{\mathbf{U}}_{st}^\mu \right\|_{\mathbf{X}_{st,st}} &\leq C^{-1} \left(\chi^L \|\mathbf{L}_{s,t\mu}\|_F \left\| \mathbf{X}_{st,st}^{-1/2} \right\|_2 + \chi^K \|\mathbf{K}_{s,t\mu}\|_F \|\mathbf{X}_{st,st}^{-1}\|_2 \left\| \widehat{\mathbf{U}}_{st}^\mu \right\|_{\mathbf{X}_{st,st}} \right) \sqrt{d+1} \varepsilon \\ &\quad + C^{-1} \left\| \widehat{\mathbf{L}}_{st}^\mu - \widehat{\mathbf{K}}_{st,st}^\mu \widehat{\mathbf{U}}_{st}^\mu \right\|_{\mathbf{X}_{st,st}^{-1}}. \end{aligned} \quad (43)$$

Proof. See the proof in [3], Theorem 1. The only difference lies in the additional $\sqrt{d+1}$ factor in the TT-MDEIM error estimate, which is due to the fact that we are considering a TT basis for the residuals and Jacobians. \square

We refer to [3] for additional details. Here, we just remark that the estimate in (43) comes across as conservative, since not all the quantities appear to be decaying with ε . In practice, however, the residual-like quantity $\left\| \widehat{\mathbf{L}}_{st}^\mu - \widehat{\mathbf{K}}_{st,st}^\mu \widehat{\mathbf{U}}_{st}^\mu \right\|_{\mathbf{X}_{st,st}^{-1}}$ is closely linked to ε . Indeed, when dealing with reducible problems according to the definition in [4], if the reduced subspace is properly constructed (i.e. the parameter sampling procedure needed to collect the snapshots is appropriate), this residual exhibits the same behavior as the estimate in (17). In our practical applications, we empirically prove that the error of the method is indeed proportional to ε .

5. LINEAR ELASTICITY EQUATION

In this section, we briefly discuss the FOM and TT-RB implementation in the case of an unsteady, parameterized linear elasticity equation. For any $\mu \in \mathcal{D}$, the strong form of the problem reads as

$$\begin{cases} \frac{\partial \underline{u}^\mu}{\partial t} - \nabla \cdot (\underline{\underline{\sigma}}^\mu(\underline{u}^\mu)) = \underline{0} & \text{in } \Omega \times (0, T], \\ \underline{u}^\mu = \underline{g}^\mu & \text{on } \Gamma_D \times (0, T], \\ \underline{\underline{\sigma}}^\mu(\underline{u}^\mu) \cdot \underline{n} = \underline{h}^\mu & \text{on } \Gamma_N \times (0, T], \\ \underline{u}^\mu = \underline{u}_0^\mu & \text{in } \Omega \times \{0\}. \end{cases}$$

The main difference with respect to (7) is that the unknown of the problem is a displacement, and as such it assumes vector-values instead of scalar values; we also define the stress tensor

$$\underline{\underline{\sigma}}^\mu(\underline{u}^\mu) = 2p^\mu \underline{\underline{\epsilon}}(\underline{u}^\mu) + \lambda^\mu \nabla \cdot (\underline{u}^\mu) \underline{I}.$$

Here $\underline{\underline{\epsilon}}$ indicates the symmetric gradient operator, and λ^μ, p^μ are the Lamé coefficients one can express as functions of the Young modulus E^μ and the Poisson coefficient ν^μ as

$$\lambda^\mu = \frac{E^\mu \nu^\mu}{(1 + \nu^\mu)(1 - 2\nu^\mu)}; \quad p^\mu = \frac{E^\mu}{2(1 + \nu^\mu)}.$$

Upon defining the vector-valued Hilbert spaces for the spatial FE discretization

$$\mathcal{V} = (H^1(\Omega))^d; \quad \mathcal{V}_{\Gamma_D}^0 = \{ \underline{v} \in (H^1(\Omega))^d : \underline{v} = \underline{0} \text{ on } \Gamma_D \},$$

we proceed in a similar fashion as in Sect. 3 to derive the space-time FOM for the elasticity problem, which reads

$$\mathbf{K}_{st,st}^\mu \mathbf{U}_{st}^\mu = \mathbf{L}_{st}^\mu. \quad (44)$$

We remark that (44) is in essence analogous to the FOM associated to the previously discussed heat equation. Therefore, we can employ the ROM equation (14) just as before. In fact, the ST-RB formulation for the elasticity problem is identical to that of the heat equation. On the other hand, we must tweak TT-RB to account for the vector-valued nature of the elasticity problem. In fact, in order to write the snapshots in the ‘‘split-axes’’ format is to introduce a new axis that collects the components of the displacements. In other words, we consider as snapshot tensor

$$\mathbf{U}_{1,\dots,d,c,t,\mu} \in \mathbb{R}^{N_1 \times \dots \times N_d \times N_c \times N_t \times N_\mu},$$

where the subscript c stands for ‘‘component’’, and N_c denotes the number of components in the vector field ($N_c = d$ in this problem). This implies that the TT decomposition for the displacement features an additional $3d$ core, that serves as a low rank approximation for the component axis:

$$\Phi_{st,\hat{t}} = \Phi_{\hat{0},1,\hat{1}} \cdots \Phi_{\widehat{d-1},d,\hat{d}} \Phi_{\widehat{d},c,\hat{c}} \Phi_{\widehat{c},t,\hat{t}}.$$

Similarly, the hyper-reduction for the residuals/Jacobians will return the TT decompositions

$$\left\{ \Phi_{\hat{0},1,\hat{1}}^L, \dots, \Phi_{\widehat{d-1},d,\hat{d}}^L, \Phi_{\widehat{d},c,\hat{c}}^L, \Phi_{\widehat{c},t,\hat{t}}^L \right\}; \quad \left\{ \Phi_{\hat{0},1,\hat{1}}^K, \dots, \Phi_{\widehat{d-1},d,d,\hat{d}}^K, \Phi_{\widehat{d},c,c,\hat{c}}^K, \Phi_{\widehat{c},t,\hat{t}}^K \right\}.$$

As a consequence, the Galerkin projection procedure detailed in Subsection 4.4 increases by one step, due to the presence of the additional component core.

6. NUMERICAL RESULTS

In this section, we investigate the numerical properties of the proposed TT-RB method presented in Sect. 4. As test cases, we firstly consider a heat equation with parameterized Dirichlet datum, forcing term, and conductivity coefficient. Secondly, we consider an unsteady linear elasticity equation, with parameterized Young modulus, Poisson coefficient, and Neumann datum. In our tests, we compare the performance of our proposed method with that of the standard ST-RB method, for different tolerances ε and mesh sizes h . In particular:

- *Offline performance*: we empirically demonstrate the efficiency TT-RB achieves with respect to ST-RB, both when computing the reduced subspace and when running the hyper-reduction step. In addition, we empirically verify the claims regarding the accuracy of TT-MDEIM made in Subsection (4.2).
- *Online performance*: we measure and compare the error and the computational gains the ST-RB and TT-RB achieve with respect to the HF solutions, checking the correctness of the accuracy estimate (43). For this purpose, we consider several tolerances $\varepsilon \in \mathcal{E} = \{10^{-2}, 10^{-3}, 10^{-4}\}$.

For both tests, we run the simulations on a fixed geometry, namely $[0, 1]^3$ for the first test, and $[0, 1] \times [0, 1/3]^2$ for the second one. The time marching algorithm we employ is the Crank Nicolson scheme. We also consider a fixed temporal domain $[0, 0.15]$, discretized with a time step of $\delta = 0.0025$, and thus $N_t = T/\delta = 60$. We select the disjoint sets of offline and online parameters $\mathcal{D}_{off} = \{\mu_k\}_{k=1}^{N_\mu}$, $\mathcal{D}_{on} = \{\mu_k\}_{k=1}^{N_{on}}$ according to a uniform distribution on \mathcal{D} , with

$N_\mu = 50$ and $N_{on} = 10$. We use \mathcal{D}_{off} to construct the reduced subspaces, and only the first 30 parameters of \mathcal{D}_{off} to obtain the TT-MDEIM approximations. We evaluate the accuracy of the methods according to

$$E = \frac{1}{N_{on}} \sum_{i=1}^{N_{on}} \frac{\|\widehat{U}_{st}^{\mu_i} - U_{st}^{\mu_i}\|_{\mathbf{X}_{st,st}}}{\|U_{st}^{\mu_i}\|_{\mathbf{X}_{st,st}}}.$$

For both tests, we consider the spatial norm matrix $\mathbf{X}_{s,s}$ defined in (10), and $\mathbf{X}_{st,st}$ is a block-diagonal matrix with N_t blocks $\delta \mathbf{X}_{s,s}$, as mentioned in Sect. 3. To evaluate the computational cost of ST-RB and TT-RB, we consider the speedup they achieve with respect to the HF simulations. The speedup is defined as the ratio between the HF cost, in terms of either wall time or memory footprint, and the ROM cost. We also introduce the reduction factor that our ROMs achieve, defined simply as the ratio between the FOM dimension N_{st} and the dimension of the reduced subspace (i.e. r_{st} for ST-RB, and r_t for TT-RB). All the numerical tests are run on a local computer with 66Gb of RAM and an Intel Core i7 running at 3.40GHz. The simulations are run using our ROM library developed in the `Julia` programming language, developed in close collaboration with Gridap [35, 36], a package for the numerical approximation of PDEs.

6.1. Heat equation. In this part, we solve the heat equation introduced in Sect. 3, and characterized by the following parametric data:

$$\alpha^\mu(\underline{x}, t) = e^{x_1 \sin(t)^2 / \sum_i \mu_i}; \quad g^\mu(\underline{x}, t) = e^{-x_1/\mu_2} |1 - \cos(9\pi t/5) + \sin(9\pi t/5\mu_3)|; \quad f^\mu(\underline{x}, t) = \sin(9\pi t/5\mu_3),$$

where $\boldsymbol{\mu} = (\mu_1, \mu_2, \mu_3)^T \in [1, 10]^3$. We define Γ_D as the side faces of Ω , whereas we impose a homogeneous Neumann condition on the top and bottom. We consider a homogeneous initial condition. In space, we employ a isotropic discretization by means of $Q2$ Lagrangian elements. The information related to the HF simulations are presented in Tb. 1.

	$h = 1/8$	$h = 1/10$	$h = 1/12$
N_s	3375	6859	12167
WT (s)	5.91	14.66	35.63
MEM (Gb)	2.99	7.13	14.18

TABLE 1. Details of the HF simulations, heat equation. From top to bottom: spatial number of DOFs, average wall time, and average memory allocations of a HF simulation.

Next, in Tb. 2 we compare the cost of running the offline phase of ST-RB and TT-RB. Since the offline cost of ST-RB is essentially agnostic to the tolerance, we only show the results obtained with $\varepsilon = 10^{-4}$. The same cannot be said in general for TT-RB, since the computational cost of running each step in the TT-SVDs depends on the size of the core found at the previous iteration. Therefore, the cost measures we present in this case are intervals, with the lower bound always being the estimate found considering $\varepsilon = 10^{-2}$, and the upper bound with $\varepsilon = 10^{-4}$.

	Measure	Basis construction			Hyper reduction		
		$h = 1/8$	$h = 1/10$	$h = 1/12$	$h = 1/8$	$h = 1/10$	$h = 1/12$
STRB	WT (s)	15.86	22.32	39.66	13.37	21.12	35.77
	MEM (Gb)	0.90	1.59	2.61	8.59	17.13	30.65
TTRB	WT (s)	[1.62, 1.85]	[3.06, 3.42]	[5.23, 5.90]	[6.30, 6.31]	[13.03, 13.06]	[24.13, 25.71]
	MEM (Gb)	[1.12, 1.36]	[2.10, 2.46]	[3.51, 4.24]	[2.31, 2.34]	[4.66, 4.71]	[8.23, 8.26]
TTRB*	WT (s)	[0.54, 0.62]	[1.03, 1.12]	[1.79, 1.94]	[6.26, 6.26]	[13.05, 13.08]	[24.06, 24.12]
	MEM (Gb)	[0.38, 0.44]	[0.70, 0.80]	[1.17, 1.39]	[2.31, 2.44]	[4.66, 4.70]	[8.24, 8.26]

TABLE 2. Offline results, heat equation. From left to right: wall time and memory allocations relative to the construction of the $H^1(\Omega)$ -orthogonal basis, with TPOD and TT-SVD; wall time and memory allocations relative to the the hyper-reduction, with MDEIM and TT-MDEIM. The last two rows display the results obtained imposing $L^2(\Omega)$ -orthogonality of the TT-RB basis. The results relative to ST-RB are obtained with $\varepsilon = 10^{-4}$, while for TT-RB we display the lower and upper bounds for every $\varepsilon \in \mathcal{E}$.

In terms of wall time, TT-RB outperforms ST-RB by a factor $\in [6, 10]$, depending on the values of h and ε . As the theoretical bounds discussed in Sect. 4 suggest, the speedup that TT-SVD achieves appears approximately constant in h (even though not all the assumptions used to derive the bounds are satisfied in this test case, for e.g. $N_t \approx N_\mu \approx M$ does not hold). In regards to the memory consumption, TT-RB does slightly worse than ST-RB; this can be entirely explained by the reliance of TT-SVD on multiple calls to SVD functions, a fact that in general we believe dampens the benefits of

running this method. Were it possible to execute all the operations required by TT-SVD at once, as happens in TPOD (where only one large SVD is called, i.e. the spatial one), TT-SVD would appear far more performant. Nonetheless, TT-RB is highly preferable to ST-RB in terms of offline cost, also considering the cheaper hyper-reduction it performs. Additionally, we expect the speedup achieved by TT-RB to improve as $h \rightarrow 0$, for fixed values of ε . Indeed, numerical evidence suggests that the growth of the maximum rank r is subpar compared to that of $1/h$. The final two rows of Tb. 2 display the results achieved when imposing a spatial orthogonality with respect to the mass matrix, thus allowing us to use the cheaper Alg. 4 for the basis construction. The results show that this procedure is roughly ~ 3 times faster than our baseline TT-SVD, which stems from calling only 3 spatial SVDs as opposed to 9 (compare Alg. 4 with Alg. 5). On the other hand, imposing a different orthogonality condition makes little difference in terms of hyper-reduction cost, as we would expect.

We now empirically demonstrate the aptness of TT-MDEIM for the hyper-reduction of residuals and Jacobians. In the following table we compare the interpolation errors χ^L and χ^K obtained when running:

- A standard MDEIM procedure on the residual and Jacobian TT-RB bases when written as matrices (obtained by running the product (3) on the respective TT decompositions).
- The TT-MDEIM algorithm detailed in Sect. 4.

Since we empirically observed that the results are similar for every tolerance, we only show the values found when $\varepsilon = 10^{-4}$. The results show that TT-MDEIM achieves an accuracy of the same order in ε as MDEIM. One can check that the estimates are identical up to machine precision. Since we empirically reached this conclusion for every numerical experiment, we will not make the same demonstration in the subsequent linear elasticity test case to avoid redundancy.

	Measure	$h = 1/8$	$h = 1/10$	$h = 1/12$
MDEIM	χ^L	0.0937	0.0705	0.0643
	χ^K	0.0074	0.0052	0.0039
TTMDEIM	χ^L	0.0937	0.0705	0.0643
	χ^K	0.0074	0.0052	0.0039

TABLE 3. Interpolation error of MDEIM and TT-MDEIM, heat equation. From top to bottom: MDEIM, and TT-MDEIM interpolation error constants for residuals and Jacobians. The results are obtained with $\varepsilon = 10^{-4}$.

Lastly, in Tb. 4 we report the results related to the online phase.

	Measure	$h = 1/8$			$h = 1/10$			$h = 1/12$		
		$\varepsilon = 10^{-2}$	$\varepsilon = 10^{-3}$	$\varepsilon = 10^{-4}$	$\varepsilon = 10^{-2}$	$\varepsilon = 10^{-3}$	$\varepsilon = 10^{-4}$	$\varepsilon = 10^{-2}$	$\varepsilon = 10^{-3}$	$\varepsilon = 10^{-4}$
STRB	E / ε	0.53	1.83	2.24	0.40	1.90	2.29	0.37	1.63	2.20
	RF / 10^5	3.37	1.01	0.57	6.86	2.74	1.18	12.16	4.87	2.08
	SU-WT	2387.86	1891.29	1841.25	5035.22	3661.70	1883.70	15175.47	6224.11	4610.25
	SU-MEM	532.06	531.17	409.41	759.17	758.76	688.94	1301.41	1300.76	1181.69
TTRB	E / ε	0.82	2.31	6.58	0.89	2.03	4.16	3.50	1.90	2.84
	RF / 10^5	6.75	5.06	3.37	137.23	102.98	68.59	24.33	18.25	12.16
	SU-WT	2215.09	2212.65	1485.96	2839.32	2772.28	1808.27	6524.53	6092.73	4429.72
	SU-MEM	414.47	414.41	371.79	822.73	822.69	743.20	1118.74	1031.40	956.72

TABLE 4. Online results, heat equation. From top to bottom: average accuracy normalized with respect to ε ; reduction factor (in hundreds of thousands); average computational speedup in time and in memory achieved by ST-RB and TT-RB with respect to the HF simulations.

In terms of accuracy, we observe that the errors decay according to ε for both methods, with TT-RB featuring multiplicative constants that are slightly larger than those of ST-RB. These facts confirm our prior expectations, which we summarized in Thm. 4. In terms of computational cost, both methods achieve considerable speedups with respect to the HF simulations, validating their usefulness in the numerical approximation of our test case. Which ROM achieves the best performance is unclear, since the answer appears to depend on h and ε . This fact might be surprising, since TT-RB by far achieves the best reduction factor, i.e. it identifies much smaller reduced subspaces than ST-RB. The reason why this does not automatically result in a cheaper online phase is that the majority of the online cost lies in the computation of the hyper-reduction coefficients for residuals and Jacobians, according to formulas (33) for ST-RB and (34) for TT-RB. This completely masks the improved complexity reduction that the TT-SVD attains in terms of number of DOFs. However, we expect to notice decidedly improved performances for TT-RB when solving problems featuring larger Kolmogorov n -width, for example nonlinear PDEs.

6.2. Linear Elasticity Problem. We now solve an unsteady version of the linear elasticity problem solved in [4]. This problem features a Dirichlet boundary $\Gamma_D = \{0\} \times [0, 1/3]^2$ on which we impose a homogeneous condition, and three Neumann boundaries

$$\Gamma_{N_1} = \{1\} \times [0, 1/3]^2; \quad \Gamma_{N_2} = [0, 1] \times \{1/3\} \times [0, 1/3]; \quad \Gamma_{N_3} = [0, 1] \times [0, 1/3] \times \{1/3\}.$$

We consider the parametric data

$$E^\mu(t) = \mu_1 \sin(2\pi t/T); \quad \nu^\mu(t) = \mu_2 \sin(2\pi t/T); \quad \underline{h}^\mu(\underline{x}, t) = \begin{cases} \mu_3 e^{\sin(2\pi t/T)} \underline{n}_1 & \underline{x} \in \Gamma_{N_1} \\ \mu_4 e^{\cos(2\pi t/T)} \underline{n}_2 & \underline{x} \in \Gamma_{N_2} \\ \mu_5(1+t) \underline{n}_3 & \underline{x} \in \Gamma_{N_3} \end{cases},$$

and $\underline{g}^\mu(\underline{x}, t) = \underline{0}$, $u_0^\mu(\underline{x}) = \underline{0}$. The quantity \underline{n}_i indicates the normal vector in the i th direction. The parametric domain is

$$\mathcal{D} = [10^{10}, 9 \cdot 10^{10}] \times [0.25, 0.42] \times [-4 \cdot 10^5, 4 \cdot 10^5]^3.$$

Once again, we consider isotropic $Q2$ Lagrangian elements for the FE discretization. The details related to the HF simulations are shown in Tb. 5.

	$h = 1/11$	$h = 1/14$	$h = 1/17$
N_s	3234	6804	12342
WT (s)	4.86	13.59	26.15
MEM (Gb)	4.48	10.35	19.51

TABLE 5. Details of the HF simulations, linear elasticity equation. From top to bottom: spatial number of DOFs, average wall time, and average memory allocations of a HF simulation.

Next, in Tb. 6 we compare the cost of running the offline phase of our ROMs.

Measure	Basis construction			Hyper reduction		
	$h = 1/11$	$h = 1/14$	$h = 1/17$	$h = 1/11$	$h = 1/14$	$h = 1/17$
STRB WT (s)	12.43	21.08	37.93	66.28	75.66	//
MEM (Gb)	0.84	1.55	2.71	64.80	76.81	//
TTRB WT (s)	[1.50, 1.99]	[2.87, 3.86]	[5.19, 6.53]	[19.30, 21.75]	[42.45, 45.43]	[90.13, 95.05]
MEM (Gb)	[0.89, 1.25]	[1.72, 2.37]	[3.08, 3.96]	[5.77, 7.62]	[12.42, 14.62]	[22.89, 25.51]
TTRB* WT (s)	[0.50, 0.57]	[0.95, 1.22]	[1.70, 2.06]	[16.62, 18.97]	[41.24, 45.12]	[89.49, 89.50]
MEM (Gb)	[0.29, 0.37]	[0.56, 0.73]	[0.99, 1.22]	[5.07, 5.81]	[12.42, 12.46]	[22.90, 22.95]

TABLE 6. Offline results, linear elasticity. From left to right: wall time and memory allocations relative to the construction of the $(H^1(\Omega))^3$ -orthogonal basis, with TPOD and TT-SVD; wall time and memory allocations relative to the the hyper-reduction, with MDEIM and TT-MDEIM. The last two rows display the results obtained imposing $(L^2(\Omega))^3$ -orthogonality of the TT-RB basis. The results relative to ST-RB are obtained with $\varepsilon = 10^{-4}$, while for TT-RB we display the lower and upper bounds for every $\varepsilon \in \mathcal{E}$. The results relative to the ST-RB hyper-reduction with $h = 1/17$ are not displayed due to memory overflow.

In terms of basis construction, these results do not significantly differ from those presented in the heat equation. The most remarkable differences with respect to the previous test case occur during the hyper-reduction step. For every h and ε , the cost of this operation is ~ 3 times larger than in the heat equation, because of a corresponding increase of the number of nonzero entries of the Jacobian (due to the vector-valued nature of the linear elasticity problem). Most notably, this results in a phenomenon of memory overflow when running the ST-RB hyper-reduction with $h = 1/17$. Let us now consider the hyper-reduction performed by the two TT-SVDs. Even though the estimates are quite similar, there is a non-negligible difference between the two, particularly when $\varepsilon = 10^{-4}$. This difference is entirely due to a more expensive Galerkin projection of the Jacobian when imposing a $(H^1(\Omega))^3$ orthogonality of the reduced subspace. In order to properly explain this phenomenon, we present hereunder the sizes of the TT cores for both decompositions when $h = 1/17$ and $\varepsilon = 10^{-4}$:

$$r_1 = 10, \quad r_2 = 37, \quad r_3 = 37, \quad r_c = 8, \quad r_t = 8;$$

$$r_1^* = 6, \quad r_2^* = 13, \quad r_3^* = 11, \quad r_c^* = 7, \quad r_t^* = 7.$$

We notice that Alg. 5 has the effect of increasing the spatial TT ranks (despite the rank-reducing strategy presented in Sect. 4). Even though this is to be expected, what is perhaps surprising is the magnitude of the increase for low enough tolerances. This results in an increased cost associated to the Galerkin projection step, which we recall scales with r^4 , with r being the maximum rank. Fortunately, this increase has no impact on the online cost, since Alg. 5 does not affect the temporal rank (i.e. the dimension of the subspace). The increase is also far more contained for higher values of ε . This phenomenon appears also to be problem-dependent, as it was not significant in the case of the heat equation.

Lastly, in Tb. 7 we report the results related to the online phase. Note that the ST-RB results when $h = 1/17$ are missing, given the previously mentioned memory overflow.

		$h = 1/11$			$h = 1/14$			$h = 1/17$		
Measure		$\varepsilon = 10^{-2}$	$\varepsilon = 10^{-3}$	$\varepsilon = 10^{-4}$	$\varepsilon = 10^{-2}$	$\varepsilon = 10^{-3}$	$\varepsilon = 10^{-4}$	$\varepsilon = 10^{-2}$	$\varepsilon = 10^{-3}$	$\varepsilon = 10^{-4}$
STRB	E / ε	2.11	1.62	0.78	4.20	1.75	1.34	//	//	//
	RF / 10^5	3.22	1.29	0.81	6.80	2.72	1.70	//	//	//
	SU-WT	543.36	506.61	480.41	1209.18	1206.02	946.36	//	//	//
	SU-MEM	213.20	213.13	213.02	4428.54	4427.31	4425.21	//	//	//
TTTB	E / ε	29.12	18.13	16.73	24.10	19.20	27.59	51.17	16.49	16.00
	RF / 10^5	9.67	3.86	2.42	13.61	8.16	5.10	24.68	14.81	9.26
	SU-WT	557.27	515.47	512.39	1185.22	1383.68	1368.40	2024.78	2069.13	1686.99
	SU-MEM	211.70	211.69	211.68	4350.52	4350.41	4350.19	7179.29	7179.14	7178.81

TABLE 7. Online results, linear elasticity equation. From top to bottom: average accuracy normalized with respect to ε ; reduction factor (in hundreds of thousands); average computational speedup in time and in memory achieved by ST-RB and TT-RB with respect to the HF simulations. The results relative to ST-RB with $h = 1/17$ are not displayed due to memory overflow during the offline phase.

Despite an increase of the multiplicative constant, the TT-RB error still exhibits the correct convergence with respect to ε . In terms of computational abilities, we once again notice the considerable speedups with respect to the HF simulations, and the similar performance of the two ROMs despite the TT-RB achieving the highest reduction factor.

7. CONCLUSIONS AND FUTURE WORK

In this work, we propose TT-RB, a projection-based ROM which leverages the TT approximation of HF snapshots, as an alternative to standard ST-RB methods. We demonstrate by solving a heat equation and a linear elasticity problem, both on 3-cubes, that TT-RB achieves a significant offline speedup with respect to its ST-RB counterpart. The source of efficiency is primarily due to the “split-axes” format, thanks to which one can write the DOFs associated to a FE function as a tensor. One can then exploit a tensor rank-reducing strategy such as the TT decomposition, which we show is computationally cheaper than a more standard TPOD-based approach. The main novelty of the TT-RB algorithm is that it almost exclusively relies on operations whose cost scales not with the entire FOM size, but with the dimension of a single full order axis. Our method also shows the potential to achieve better online performance, given the lower dimension of the approximation subspaces compared to ST-RB. Accuracy-wise, we prove that TT-RB is characterized by the same approximation abilities as ST-RB, as we empirically demonstrate in our numerical experiments.

The most important extension of this work consists in solving parameterized problems on unstructured geometries. To this end, we plan to consider unfitted element discretizations in order to retrieve snapshots with a Cartesian structure on generic geometries. We expect this extension to not present any difficulties from a theoretical perspective, since the theory behind the algorithms presented throughout this work is agnostic from the type of discretizations and geometries we may consider.

REFERENCES

- [1] Y. Choi, P. Brown, W. Arrighi, R. Anderson, and K. Huynh. “Space–time reduced order model for large-scale linear dynamical systems with application to Boltzmann transport problems”. In: *Journal of Computational Physics* 424 (2021).
- [2] R. Tenderini, N. Mueller, and S. Deparis. “Space-Time Reduced Basis Methods for Parametrized Unsteady Stokes Equations”. In: *SIAM Journal on Scientific Computing* 46.1 (2024), B1–B32. DOI: [10.1137/22M1509114](https://doi.org/10.1137/22M1509114). eprint: <https://doi.org/10.1137/22M1509114>.
- [3] N. Mueller and S. Badia. “Model order reduction with novel discrete empirical interpolation methods in space–time”. In: *Journal of Computational and Applied Mathematics* 444 (2024), p. 115767. DOI: <https://doi.org/10.1016/j.cam.>
- [4] A. Quarteroni, A. Manzoni, and F. Negri. *Reduced basis methods for partial differential equations: an introduction*. Vol. 92. Springer, 2015.
- [5] F. Negri, A. Manzoni, and G. Rozza. “Reduced basis approximation of parametrized optimal flow control problems for the Stokes equations”. In: *Computers & Mathematics with Applications* 69.4 (2015), pp. 319–336.

- [6] G. Rozza, D. Huynh, and A. Manzoni. “Reduced basis approximation and a posteriori error estimation for Stokes flows in parametrized geometries: roles of the inf–sup stability constants”. In: *Numerische Mathematik* 125.1 (2013), pp. 115–152.
- [7] N. Dal Santo, S. Deparis, A. Manzoni, and A. Quarteroni. “An algebraic least squares reduced basis method for the solution of nonaffinely parametrized Stokes equations”. In: *Computer Methods in Applied Mechanics and Engineering* 344 (2019), pp. 186–208.
- [8] C. Prud’Homme et al. “Reliable Real-Time Solution of Parametrized Partial Differential Equations: Reduced-Basis Output Bound Methods”. In: *Journal of Fluids Engineering* 124.1 (Nov. 2001), pp. 70–80. DOI: [10.1115/1.1448332](https://doi.org/10.1115/1.1448332).
- [9] C. Prud’homme, D. Rovas, K. Veroy, and A. Patera. “A Mathematical and Computational Framework for Reliable Real-Time Solution of Parametrized Partial Differential Equations”. In: *ESAIM: Mathematical Modelling and Numerical Analysis* 36 (Sept. 2002), pp. 747–771. DOI: [10.1051/m2an:2002035](https://doi.org/10.1051/m2an:2002035).
- [10] W. Hackbusch. “Numerical tensor calculus”. In: *Acta numerica* 23 (2014), pp. 651–742.
- [11] W. Hackbusch. *Tensor spaces and numerical tensor calculus*. Vol. 42. Springer Science & Business Media, 2012.
- [12] L. R. Tucker. “Some mathematical notes on three-mode factor analysis”. In: *Psychometrika* 31.3 (1966), pp. 279–311.
- [13] I. Oseledets and E. Tyrtshnikov. “TT-cross approximation for multidimensional arrays”. In: *Linear Algebra and its Applications* 432.1 (2010), pp. 70–88.
- [14] I. V. Oseledets. “Tensor-train decomposition”. In: *SIAM Journal on Scientific Computing* 33.5 (2011), pp. 2295–2317.
- [15] A. Gorodetsky, S. Karaman, and Y. M. Marzouk. “A continuous analogue of the tensor-train decomposition”. In: *Computer Methods in Applied Mechanics and Engineering* 347 (2019), pp. 59–84.
- [16] D. Bigoni, A. P. Engsig-Karup, and Y. M. Marzouk. “Spectral tensor-train decomposition”. In: *SIAM Journal on Scientific Computing* 38.4 (2016), A2405–A2439.
- [17] S. V. Dolgov and D. V. Savostyanov. “Alternating minimal energy methods for linear systems in higher dimensions”. In: *SIAM Journal on Scientific Computing* 36.5 (2014), A2248–A2271.
- [18] S. A. Goreinov, N. L. Zamarashkin, and E. E. Tyrtshnikov. “Pseudo-skeleton approximations by matrices of maximal volume”. In: *Mathematical Notes* 62.4 (1997), pp. 515–519.
- [19] S. Badia, F. Verdugo, and A. F. Martín. “The aggregated unfitted finite element method for elliptic problems”. In: *Computer Methods in Applied Mechanics and Engineering* 336 (2018), pp. 533–553. DOI: <https://doi.org/10.1016/j.cma.2018.08.011>.
- [20] B. Unger and S. Gugercin. “Kolmogorov n-widths for linear dynamical systems”. In: *Advances in Computational Mathematics* 45.5-6 (2019), pp. 2273–2286. DOI: [10.1007/s10444-019-09701-0](https://doi.org/10.1007/s10444-019-09701-0).
- [21] P. Hansbo. “Nitsche’s method for interface problems in computational mechanics”. In: *GAMM-Mitteilungen* 28 (Nov. 2005). DOI: [10.1002/gamm.201490018](https://doi.org/10.1002/gamm.201490018).
- [22] E. Burman and P. Hansbo. “Fictitious domain methods using cut elements: III. A stabilized Nitsche method for Stokes’ problem”. In: *European Series in Applied and Industrial Mathematics (ESAIM): Mathematical Modelling and Numerical Analysis* 48 (May 2014). DOI: [10.1051/m2an/2013123](https://doi.org/10.1051/m2an/2013123).
- [23] H. Le Dret and B. Lucquin. “The Finite Element Method in Dimension Two”. In: *Partial Differential Equations: Modeling, Analysis and Numerical Approximation*. Cham: Springer International Publishing, 2016, pp. 167–218. DOI: [10.1007/978-3-319-27067-8_6](https://doi.org/10.1007/978-3-319-27067-8_6).
- [24] A. George. “Nested Dissection of a Regular Finite Element Mesh”. In: *SIAM Journal on Numerical Analysis* 10.2 (1973), pp. 345–363. DOI: [10.1137/0710032](https://doi.org/10.1137/0710032). eprint: <https://doi.org/10.1137/0710032>.
- [25] A. George and E. Ng. “On the Complexity of Sparse QR and LU Factorization of Finite-Element Matrices”. In: *SIAM Journal on Scientific and Statistical Computing* 9.5 (1988), pp. 849–861. DOI: [10.1137/0909057](https://doi.org/10.1137/0909057). eprint: <https://doi.org/10.1137/0909057>.
- [26] K. Carlberg, M. Barone, and H. Antil. “Galerkin v. least-squares Petrov–Galerkin projection in nonlinear model reduction”. In: *Journal of Computational Physics* 330 (2017), pp. 693–734.
- [27] N. Halko, P.-G. Martinsson, and J. A. Tropp. *Finding structure with randomness: Probabilistic algorithms for constructing approximate matrix decompositions*. 2010. arXiv: [0909.4061 \[math.NA\]](https://arxiv.org/abs/0909.4061).
- [28] R. Larsen. “Lanczos Bidiagonalization With Partial Reorthogonalization”. In: *DAIMI Report Series* 27 (July 1999). DOI: [10.7146/dpb.v27i537.7070](https://doi.org/10.7146/dpb.v27i537.7070).
- [29] T. Cui and S. Dolgov. “Deep composition of Tensor-Trains using squared inverse Rosenblatt transports”. In: *Foundations of Computational Mathematics* (2021), pp. 1–60.
- [30] S. Dolgov, K. Anaya-Izquierdo, C. Fox, and R. Scheichl. “Approximation and sampling of multivariate probability distributions in the tensor train decomposition”. In: *arXiv preprint arXiv:1810.01212* (2018).
- [31] S. Chaturantabut and D. C. Sorensen. “Nonlinear model reduction via discrete empirical interpolation”. In: *SIAM Journal on Scientific Computing* 32.5 (2010), pp. 2737–2764.
- [32] F. Negri, A. Manzoni, and D. Amsallem. “Efficient model reduction of parametrized systems by matrix discrete empirical interpolation”. In: *Journal of Computational Physics* 303 (2015), pp. 431–454. DOI: <https://doi.org/10.1016/j.jcp.2015.07.031>.
- [33] A. Dektor. *Collocation methods for nonlinear differential equations on low-rank manifolds*. 2024. arXiv: [2402.18721 \[math.NA\]](https://arxiv.org/abs/2402.18721).

- [34] A. Chertkov, G. Ryzhakov, G. Novikov, and I. Oseledets. *Optimization of Functions Given in the Tensor Train Format*. 2022. arXiv: [2209.14808](https://arxiv.org/abs/2209.14808) [math.NA].
- [35] S. Badia and F. Verdugo. “Gridap: An extensible Finite Element toolbox in Julia”. In: *Journal of Open Source Software* 5.52 (2020), p. 2520. DOI: [10.21105/joss.02520](https://doi.org/10.21105/joss.02520).
- [36] F. Verdugo and S. Badia. “The software design of Gridap: a Finite Element package based on the Julia JIT compiler”. In: *Computer Physics Communications* 276 (2022), p. 108341. DOI: [10.1016/j.cpc.2022.108341](https://doi.org/10.1016/j.cpc.2022.108341).